IMPROVED FABRICATION FOR MICROMIRROR ARRAYS

THESIS

Enoc Flores, Second Lieutenant, USAF

AFIT-ENG-MS-19-M-027

DEPARTMENT OF THE AIR FORCE
AIR UNIVERSITY

AIR FORCE INSTITUTE OF TECHNOLOGY

Wright-Patterson Air Force Base, Ohio

AFIT-ENG-MS-19-M-027

IMPROVED FABRICATION FOR MICROMIRROR ARRAYS

THESIS

Presented to the Faculty

Department of Electrical and Computer Engineering

Graduate School of Engineering and Management

Air Force Institute of Technology

Air University

Air Education and Training Command

In Partial Fulfillment of the Requirements for the

Degree of Master of Science in Electrical Engineering

Enoc Flores, B.S.E.E.

Second Lieutenant, USAF

March 2019

AFIT-ENG-MS-19-M-027

IMPROVED FABRICATION FOR MICROMIRROR ARRAYS

Enoc Flores, B.S.E.E.

Second Lieutenant, USAF

Committee Membership:

Maj Tod Laurvick, PhD, USAF
Chair

Dr. Hengky Chandrahalim, PhD
Member

Dr. LaVern A. Starman, PhD
Member

AFIT-ENG-MS-19-M-027

Abstract

Micromirror devices which consisted of one SU-8 2050 layer, two different exposures, and a series of metal depositions were constructed and evaluated. By varying the exposure, a micromirror structure was fabricated with different thicknesses, a ratio of 1.083 $\mu m/(\frac{mJ}{cm^2})$ was found. The initial design consisted of four layers. The pillar was made of one SU-8 layer, and the top portion had three layers in the following order: gold, SU-8, and gold. This design could not be released and did not have characteristics of a flat and conformal reflective surface. Several variations of the initial design were explored and all of them lacked a flat and conformal top reflective surface. Both interferometric and statistical software showed that using a 60 mJ/cm^2 mirror exposure dosage and a 370 mJ/cm^2 square pillar exposure dosage yields a micromirror with a conformal top reflective surface. The length and width of the pillars are 200μm by 200μm, with a height of 75 μm. The mirror's length and width are 1 mm by 1 mm, and the thickness is 65 μm. The average step height difference from the pillar to the side of the mirror, pillar to each corner of the mirror, and pillar to initial dip in the mirror is 4.53, 9.22, and 1.51 μm, respectively.

Acknowledgments

I would like to thank my adviser, Maj Laurvick, for always being available and going above and beyond to make sure all his six masters students always had everything we needed. In addition, I would have not been able to complete the class workload without the help of the MEMS Group. I would like to especially thank the Underwood brothers for always motivating me to continue going to the gym even when we were drowning in homework. Finally, I would like to thank my family for providing me with moral support throughout this journey.

Enoc Flores

Table of Contents

List of Figures

List of Tables

List of Acronyms

AFIT	Air Force Institute of Technology
AFRL	Air Force Research Lab
CZ	Czochralski Growth
DUV	Deep Ultraviolet
HF	Hydrofluoric Acid
IC	Integrated Circuit
LPCVD	Low-Pressure Chemical Vapor Deposition
MED	Mirror Exposure Dose
MEMS	Micro-Electro-Mechanical Systems
PEB	Post Exposure Bake
PED	Pillar Exposure Dose
SiO_2	Silicon Dioxide
SLL	Single Layer Liftoff
UV	Ultraviolet

MEMS MICROMIRRORS

1. Introduction

Microelectromechanical systems (MEMS) is a unique field of study that incorporates physics, chemistry, electrical, and mechanical effects simultaneously. As the years progress, these micro scale devices are becoming more complex and sophisticated. For the most part MEMS devices are used for actuation and sensing purposes. These small devices are incorporated into our everyday lives and are even used to maintain national security. A few examples include, televisions, computers, cell phones, advanced military systems, and space vehicles. Each design requires different specifications, constraints, and fabrication methods. Overall, MEMS can have simple stationary components or complex structures that mechanically move [1], [2]. In the lab, standards of cleanliness need to be excellent and meticulous efforts need to be taken to ensure proper fabrication of MEMS devices.

Today's aircraft beam steering technology poses various problems that include unwanted turbulence, vibrations, and weight. As a result, the U.S. Air Force is looking into replacing this outdated technology with MEMS. Typically, a beam steering device consists of an array of mirrors that can move via actuators. This type of device is desired by the U.S. Air Force since it can be used to reflect any type of photon emission [3].

Continuing with prior efforts from the Air Force Research Laboratory (AFRL) and the Air Force Institute of Technology (AFIT), the goal of this research is to fabricate a low mass, sturdy, and optically flat micromirror that will be used in the electrostatically actuated bimorph structures, which are also easier to fabricate when compared to flip chip bonding used up to this point. To that end, structures made from SU-8 were investigated. Fabrication of these devices is somewhat an art, which makes replicating structures in the clean room a difficult task; therefore,

laying out a detailed process sheet that is easy to follow would be beneficial for future use. Final micromirror devices consist of one SU-8 2050 layer, two different exposures, and a series of metal depositions. The length and width of the pillars are 200μm by 200μm, and the height is 75 μm. The mirror's length and width are 1 mm by 1 mm, and the thickness is 65 μm. The average step height difference from the pillar to the side of the mirror, pillar to each corner of the mirror, and pillar to initial dip of the mirror is 4.53, 9.22, and 1.51 μm, respectively.

2. Background

The following section will provide the required literature and background to obtain a basic understanding of the previous work done by researchers at AFRL and AFIT [2]–[5]. In addition, this section will focus on the concepts and physics needed to understand integrated circuit (IC) fabrication techniques and processes that are related to this research.

2.1 MEMS Overview

MEMS are micrometer scale systems that are made up of moving and electrical parts that can be built for unique applications. Depending on more specific needs for each application, MEMS devices have been able to branch out into other fields such as, microoptoelectromechanical systems for optical applications, radio frequency MEMS for radio-frequency applications, and nanoelectromechanical systems if the system includes at least one component less than 1 μm. Finally, if MEMS are used in a biological application, then that system is referred to as bioMEMS [6].

2.1.1 MEMS History

It was not until the 1960s that researchers realized that IC processing could be used in dynamic ways by taking full advantage of all the properties that silicon has to offer. Traditionally, IC fabrication only focuses on the electrical properties of silicon, but MEMS devices use both electrical and mechanical properties of silicon. Depending on how silicon is fabricated, it can exhibit flexible membranes characteristics. Changes in pressure can move this type of silicon material, which allows it to be electrically measured. This type of device is known as a pressure sensor. After the discovery of MEMS sensors came the development of MEMS actuators. MEMS actuators are microscale devices that actuate when an electrical input is properly applied to the system [7].

2.1.2 MEMS Uses

A transducer is a substance or a device that converts input energy into a different output energy. This is known as a sensor or actuator. Transducers have a broad definition because they are used in many applications. Examples of common transducers include microphones, solar cells, incandescent light bulbs, electrical motors, and even human beings [5].

2.1.2.1 Actuators

A device that moves or moves something is known as an actuator [5]. Common physical stimulus that create actuation in MEMS devices are electric fields, magnetic fields, and thermal effects. Actuation via electric fields include electrostatic and piezoelectric. Displacement by magnetic fields include magnetostatics and magnetostrictive. Finally, thermal actuation involves the difference between thermal coefficients of expansion of two materials [7].

Electrostatic actuation occurs when an electric field is created between two adjacent conductors. One of the most basic examples of electrostatic actuation is a cantilever beam used to deflect a laser beam. The cantilever beam in this example is used as an optical switch and can be seen in Figure 1. Voltage is applied to the electrode that has an insulating $Si0_2$ layer separating the substrate from the electrode. The silicon substrate that is directly attached to the conducting polysilicon cantilever beam is grounded. As a result, an electric field is created that generates a small force that deflects the tip of the cantilever beam downward. The forces are in the nanonewton to micronewton range [7].

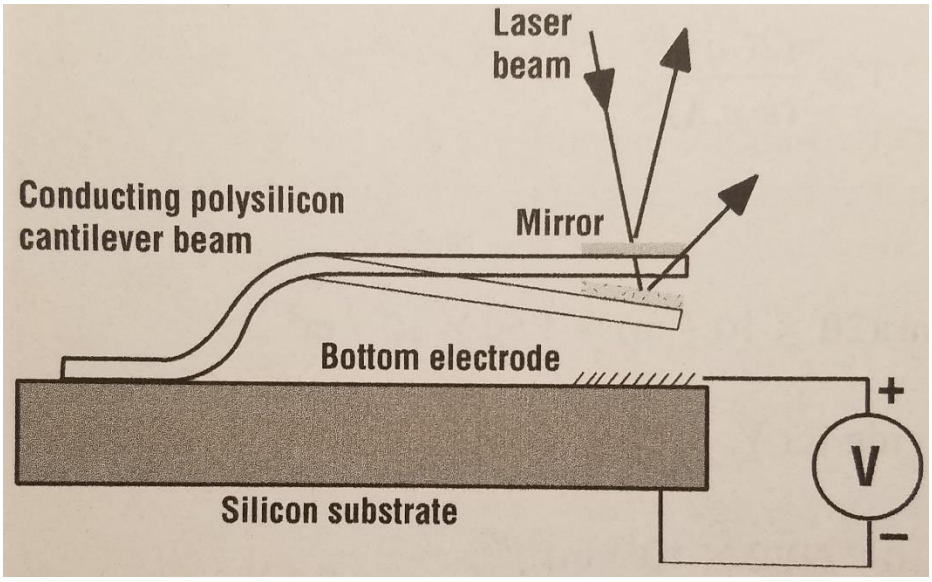

Figure 1: Electrostatic actuation of a cantilever beam [7].

2.1.2.2 Sensors

A sensor converts a physical quantity to an electrically measurable parameter. In other words, it is a device that can electrically measure a change in resistance, capacitance, or oscillation frequency when it properly undergoes a change in pressure, acceleration, or mass change [7].

A common example of a sensor involves the piezoelectric effect. An electrical charge is generated on the surface of a piezoelectric material when it undergoes a force that compresses it. A charge is generated because the applied force creates stress that turns into strain. Strain then creates electric dipoles that induce surface charges to finally create an electric field [7].

2.1.3 Advantages of MEMS

MEMS devices have been of high interest in the scientific and engineering communities due to the many advantages they have to offer. Some of those advantages include small size, performance, batch fabrication, cost-effective integration with electronics, and a significant

reduction in power consumption [8]. Since MEMS devices operate on the microscale, they are sought out in applications where minimizing weight and size are of an essence. Finally, MEMS can be a more affordable alternative to IC manufacturers since they can be made in large batches using a single design yielding high throughput [3].

2.2 Materials

Conductors, semi-conductors, and insulators are used in both IC and MEMS fabrication. Each layer is patterned one layer at a time during fabrication. The electrical and mechanical properties are designed and built to meet unique specifications that will enable a certain function, but selection is based on both the requirements of the final product as well as the ability to selectively remove sacrificial material and leave the desired material [3].

2.2.1 Conductors, Semi-Conductors, and Insulators

The locations of the energy bands in the band diagram determine the characteristics of a given material. Energy bands can overlap or form gaps, and if a bandgap is present the size of it provides further details about the material. Band diagrams usually consist of a valance band (bottom band) and a conduction band (top band). Electrons move from the valance band to the conduction band, and holes move and start in the opposite way. A bandgap will not be present in a material that is conductive. This allows electrons to freely move into the conduction band upon excitement. Insulators have a large bandgap between the conduction band and the valance band, which makes it difficult for electrons to travel to the conduction band. Finally, semiconductors fall in between insulators and conductors where a bandgap is present, but the gap is small where electrons can still travel to the conduction band. The bandgap for silicon at a temperature of 300 K is 1.124 eV [9].

2.2.2 Important Materials for MEMS

According to the PolyMUMPs design handbook, common materials used to fabricate MEMS devices are single-crystal silicon, poly-crystalline silicon, silicon dioxide, silicon nitride, and metal [10]. The subsections that follow will summarize the basic characteristics of each material.

2.2.2.1 Single-Crystal Silicon

In the periodic table, silicon is in the group IV elements. Silicon has "four valence electrons and needs four more electrons to complete its valence shell" [7]. To complete its valence shell silicon needs to form covalent bonds with four nearest neighbor atoms. When this is achieved a single crystalline structure is created and it is also referred to as a diamond structure. In addition, the single crystalline structure can be thought of as two interlocking FCC lattices that are offset by $(a/4, a/4, a/4)$ [7].

Wafers are the backbone of MEMS devices since it is where devices are fabricated on. The most common technique used to grow single-crystal silicon wafers is called Czochralski growth (CZ). From the CZ growth yields a large boule that is later sliced into thin wafers and used as a semiconductor. Silicon boules can reach diameters of over 300 mm and 1 to 2 m long. The CZ growth consists of submerging a single crystal 'seed' into a melt and slowly pulling it out, allowing solidification, while rotating it counter clockwise [7].

2.2.2.2 Poly-Crystalline Silicon

Many individual single crystalline silicon structures make up poly-crystalline silicon, which is also known as polysilicon. The difference between the two is that the crystalline silicon structures in polysilicon are not perfectly aligned with each other. This means that polysilicon is

not a lattice matched structure and single crystalline silicon is. Growing single crystal ingots with minimal crystal defects is already a challenging task; therefore, the choice of using polysilicon as the preferred material in deposition techniques facilitates the process of making MEMS devices. Low pressure chemical vapor deposition (LPCVD) is the most common way to deposit polysilicon onto silicon wafers and is done at a temperature of 600^{o}C. Polysilicon is the most common material that serves as a structural material in MEMS devices and is typically 1 to 2 μm thick [7]. The electrical properties of both single crystal silicon and polysilicon can be altered by adding accepter or donors, which is known as P or N type doping, respectively [9].

2.2.2.3 Silicon Dioxide

In a previous example involving an actuating cantilever beam, silicon dioxide (SiO_2) was used as an insulating layer to separate two conductive layers. Silicon dioxide can be used as an insulating material because it has a bang gap of 8.9 eV [9]. In other MEMS applications, silicon dioxide is commonly used as a sacrificial layer due to two desirable properties. First, it can withstand the 600^{o}C LPCVD deposition temperature of polysilicon. Finally, silicon dioxide has a faster hydrofluoric acid (HF) etch rate than polysilicon. In addition, when silicon dioxide is doped with phosphorus, forming phosphosilicate glass, its HF solution etch rate is 8 to 10 times faster than undoped silicon dioxide. This selectivity makes it a good sacrificial material when silicon structures are to be made [7]. It is also important to note that silicon exposed to oxygen at room temperature will begin to yield silicon dioxide [3].

2.2.2.4 Silicon Nitride

MEMS devices can also use silicon nitride as an insulator. Its benefit over silicon dioxide is its resistance to oxidize. As a result, silicon nitride is commonly used in MEMS devices as an

electrical isolation between the polysilicon and the substrate. Due to its high strength it can also be used as a layer in the device [3], [10].

2.2.2.5 Metal

Metal is a conductor and is typically used to make electrical contacts in MEMS devices [9], [10]. Metals are used in solar cells, thin film batteries, and many other technologies [7]. All kinds of metals are used in MEMS; however, for the purposes of this research only gold, platinum, chrome, and aluminum will be discussed since they will be used to fabricate micromirrors [10].

2.3 Fabrication

The sections that follow will cover the processes and techniques used to fabricate MEMS devices. Specifically, the processes and techniques used to fabricate micromirrors, in this research, and the previous work done by AFIT.

2.3.1 Photolithography

Photolithography, one specific kind of lithography, is one of the most important fundamental processes used to make ICs and MEMS devices [7], [10]. Lithography is important because it "encompasses all the steps involved in transferring a pattern from a mask to the surface of the silicon wafer" [11]. Photolithography starts by coating a wafer with photoresist. Depending on the step of fabrication, a mask and wafer are aligned via alignment marks. Then the pattern is transferred onto the wafer when the photoresist is exposed with either visible, ultraviolet (UV), or deep ultraviolet (DUV) light (Figure 2). It is a useful process because masks can be used multiple times. Masks transfer designs onto wafers in a specific way, depending on

the type of photoresist being used, by blocking or allowing a light source to reach the photoresist [7], [10].

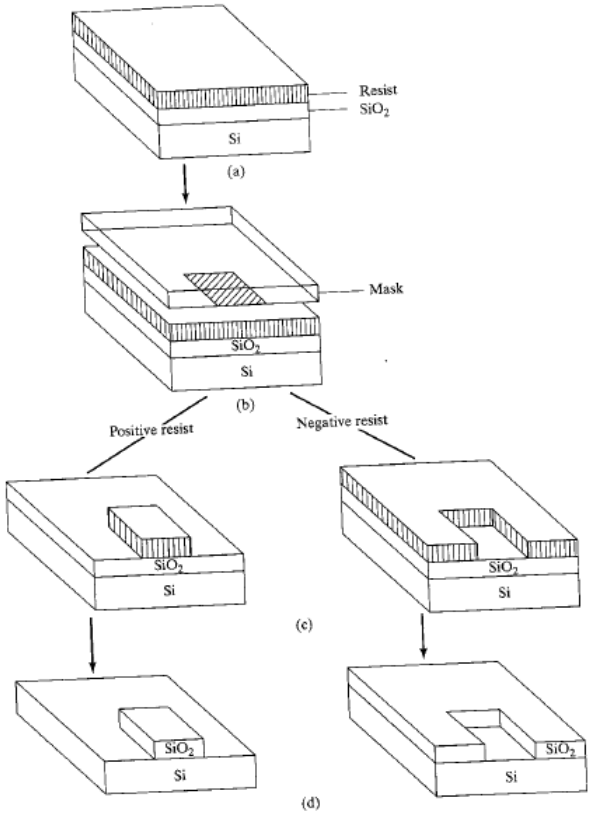

Figure 2: Photolithography steps: cover substrate with photoresist, align mask with substrate, expose substrate with a light source, develop photoresist, etch pattern, and remove the remaining photoresist [11].

Mask creating starts by determining what layers are needed, then laying out features. The next step is to generate models which might run through 3D finite element analysis modeling. Each modeling software is different; therefore, it is important to consult the layout rules to ensure compliance. Typically, each layer in the fabrication process requires a mask. Masks are fabricated on fused silica that have a bottom chromium layer and a layer of photoresist on top. Mask making technology allows specific files to be uploaded onto machinery and using a process like photolithography, pattern a mask. After the mask has been patterned and developed,

the exposed chromium is etched away yielding a mask that can be used to pattern wafers [7]. For this research the MEMS L-Edit v8.3 will be used to create masks.

2.3.2 Photoresist

Following mask and wafer alignment, high-intensity UV light is used to expose the top photoresist layer, also known as resist, and change the properties of that material [11]. "Multiplying the intensity by the exposure time provides the [exposing radiation] dose (J/cm^2) [7]." Depending on the application and thickness of the resist layer, radiation doses should be properly changed.

Typically, a wafer is coated with resist via spin coating. The wafer is first placed on top a vacuum chuck that tightly holds the wafer in place with a vacuum [7]. About 1 ml of resist for each inch of substrate diameter is dispersed on the wafer. Then depending on the desired thickness of the photoresist layer one would set a spin speed, acceleration, and time to uniformly spread the resist on the wafer. Thickness vs spin speed for various SU-8 2000 resists can be seen in Figure 3 [12]. Following resist application, the wafer undergoes a soft bake followed by UV exposure. Depending on the type of photoresist, positive or negative, the lithography steps to completion differs [7], [11].

Shipley's 1818 is an example of a positive resist. After exposure, it is common to develop the resist. In this step, the parts that have been exposed to UV light will wash away when it encounters developer solution. The opposite is true in the case of negative resist. In other words, the areas that have been exposed to UV light will remain after development. For the case of SU-8 resist, which will be used in this research, a post exposure bake (PEB) must take place directly

after exposure. After a PEB the wafer can be developed. The development time and baking temperatures vary for different thicknesses and photoresists [12].

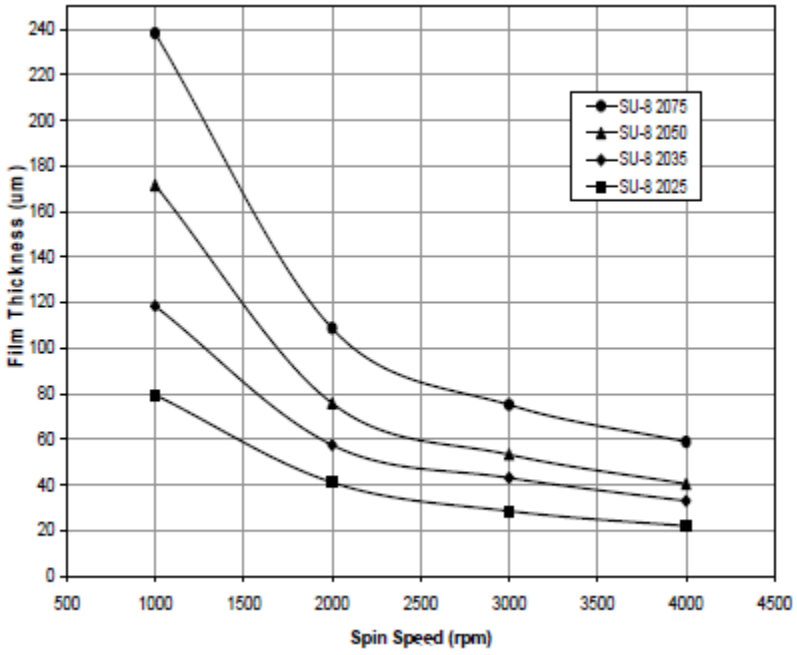

Figure 3: Spin speed vs film thickness for selected SU-8 2000 resists [12].

2.3.3 Surface Micromachining and Etching

Surface micromachining is a process that takes place on the surface of the wafer. “Films used for structural elements are deposited using techniques such as LPCVD”. Several layers can be deposited to make up a structure. Some of those layers are later removed through etching to allow motion of the structural layer. Polysilicon is the most common surface micromachining structural material due to its ability to be “deposited with well-controlled, repeatable film stress levels”. In addition, polysilicon is also isotropic which can be an advantage in some structures [7]. Bulk micromachining, essentially the opposite of surface micromachining, is another method to fabricate MEMS devices, but this research will only utilize surface micromachining.

Following the completion of photolithography, the next step involves etching. Wet chemical etching involves the submersion of a wafer into a "solution that reacts with the exposed film to form soluble by-products." This method is typically undesired since it is "difficult to control, is prone to high defect levels due to solution particulate contamination, cannot be used for small features, and produces large volumes of chemical waste." Dry and plasma etch process are better than wet etching [7]. It is also important to note different techniques, materials, and solutions will either etch a material uniformly in all directions, isotropic etch, or only in one, anisotropic etch. Overall, wet chemical etching is an isotropic process [11].

2.3.4 Liftoff

An alternative to wet etching is liftoff. This method involves patterning a thick layer of resist. A thick layer is about 2 μm. Then it is common to evaporate a thin layer of metal, which can be a couple hundred nanometers. The areas where metal is on top of resist lifts off of the wafer as the resist dissolves in developer or acetone. An ultrasonic agitation bath can be used to accelerate liftoff [7]. This method and a variation of it will be used in this research.

2.3.5 Sputtering

In microelectronic fabrication metal thin films are usually deposited via evaporation; however, sputtering is the primary alternative for thin film deposition. Sputtering "has better step coverage than evaporation, induces far less radiation damage than electron beam evaporation, and is much better at producing layers of compound materials and alloys [7]." This research will use sputtering as the preferred method to deposit metal layers since it is accessible.

Figure 4 shows an image of a basic sputtering system. It consists of a parallel-plate plasma reactor in a vacuum chamber. "The plasma chamber must be arranged so that high energy

ions strike a target containing the material to be deposited" onto the wafer. The cathode and anode are closely spaced to ensure that as many of these ejected atoms are collected. The pressure in the chamber is held at about 0.1 $torr$ and an inert gas is normally used to supply the chamber [7].

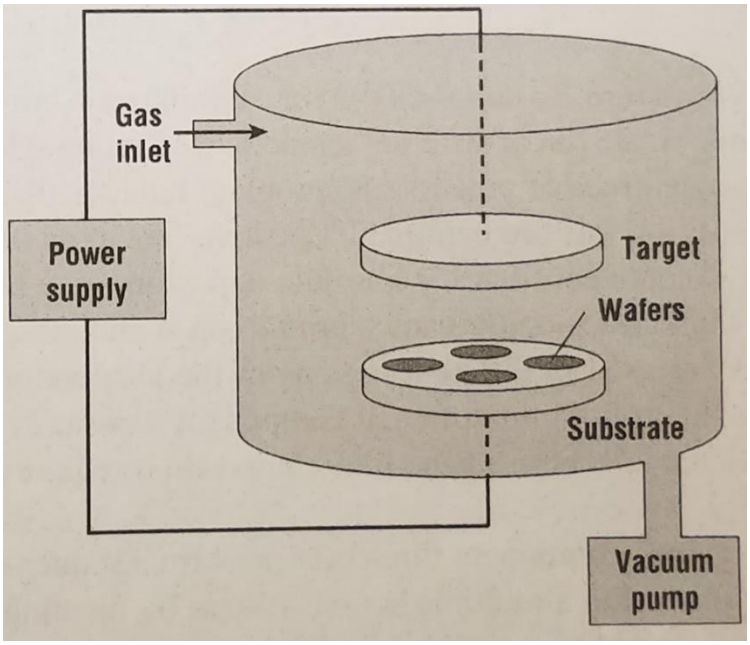

Figure 4: Chamber for a simple parallel-plate sputtering system [7].

2.3.6 Multi-User MEMS Processes

The Multi-User MEMS Processes (MUMPs) is a commercial program that fabricates MEMS devices. They have three different processes: PolyMUMPs, MetalMUMPs, and SOIMUMPs. PolyMUMPs is a three-layer polysilicon surface micromachining process that was used to fabricate electrostatically actuated bimorph beam structures that this research builds on.

2.3.6.1 PolyMUMPs Process Overview

The PolyMUMPs fabrication process is done on a silicon substrate. The order and layers that are deposited are as follows: nitride, Poly0, 1st Oxide, Poly1, 2nd Oxide, Poly2, and Metal.

Each layer's thickness varies from 0.5 μm to 2.0 μm. Surface materials are deposited by LPCVD. The nitride layer is used to provide electrical isolation from water. The oxide layers are made up of phosphosilicate glass and usually serve as sacrificial layers. They too help define the gaps between structural layers. Poly0 is typically used as an electrical layer for ground plane/electrode formation. Poly1 and Poly2 are the first and second mechanical layers, respectively. Finally, the metal layer is used as an electrical contact layer or for optical reflective purposes [10].

All layers are patterned using photolithography techniques and etched using reactive ion etching. The final gold metal layer is deposited and patterned using a standard liftoff technique. At the end a release etch is done by immersing the silicon wafer in hydrofluoric acid for 2-3 minutes. This gets rid of the sacrificial layers and frees both Poly1 and Poly2 [10]. Figure 5 shows a cross section view of the PolyMUMPs process.

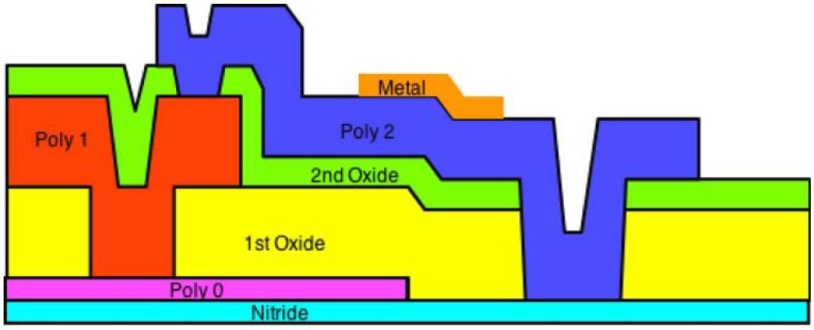

Figure 5: Cross section view of the PolyMUMPs process [13].

2.3.7 Previous Micromirror Research

AFRL and alumni of AFIT have modeled and tested electrostatically actuated bimorph beam structures for use in a micromirror array. This platform is being actuated with a new electrostatic "zipper" actuation scheme. Essentially, this design consists of stacking bimorph

cantilever beams in such a way that allows for the deflections of each beam to be added together. The “zipper” structure is then actuated by applying a voltage to an electrode on the bottom of the cantilever beams [14]. To have more control of the actuation phenomena, the electrodes on the bottom of the beams have been segmented. This in turn allows only one or various parts of the beam to be pulled in and in turn pull other connected beams, opposed to being constricted to only pulling the whole “zipper” beam [15]. The micromirror will sit on top of a platform that has four “zipper” beams on each side. Overall, their research found that the pull-in and displacement behavior of a bimorph beam changes as the electrode configuration changes [3]. Figure 6 shows the L-Edit layout of the micromirror platform. L-Edit files are sent to PolyMUMPs for fabrication.

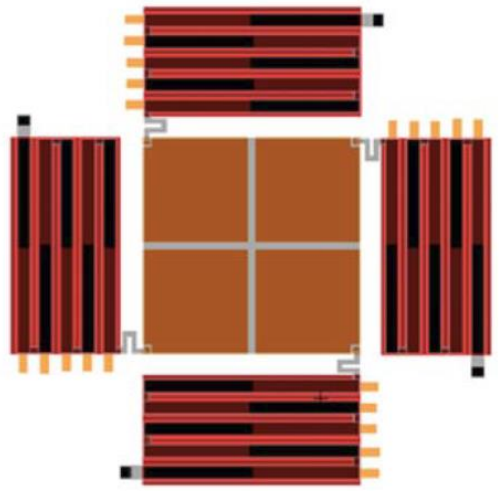

Figure 6: Actuation platform layout created on L-Edit [3].

Current researchers at AFRL fabricated a MEMS deformable mirror device of excellent optical quality with roughness of the entire area of 15.1 nm, bowed slightly upward between ±40 and ±70 nm. Fabrication consisted of first spinning on a 3 μm SU-8 2002 photoresist layer to serve as an etch stop layer. Then 100 nm of gold was electron beam evaporated, followed by an

additional SU-8 2002 250 nm layer that was encapsulated by an evaporated 100 nm gold layer. Finally, a 250 nm thick layer of unexposed SU-8 2002 was used to bond the mirror wafer to the detector wafer. These devices are tough to make and difficult to replicate; therefore, this research will attempt to simplify the process to facilitate replication and add a pillar to the structure without bonding requirements [4].

2.4 Improving MEMS Micromirror Fabrication

Silicon MEMS micromirrors are undesirable, at least in this application, because they are heavy and need to be flip chip bonded onto the micromirror actuator array platform. Flip chip bonding is done with an epoxy material that sticks the micromirror to the platform and can be seen in Figures 7 and 8. This process is not perfect and varies from one device to the other since it is done by hand. As a result, the final product will have an undesirable tilt that may lead to collisions between adjacent mirrors and a low yield. Regardless of the micromirror placement, the heavy weight of the silicon micromirror will inhibit ideal functionality of the device.

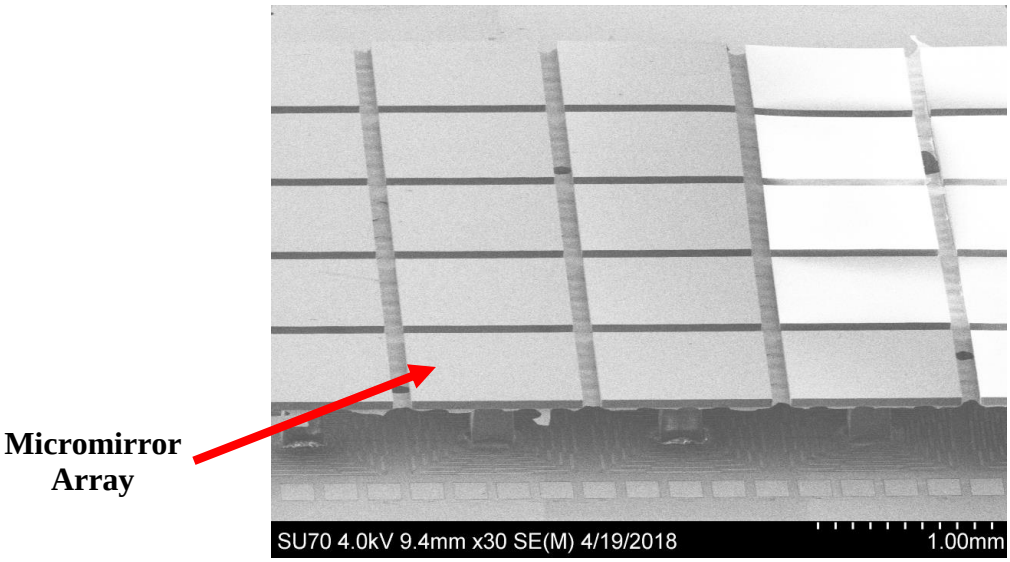

Figure 7: Image of flip chip bonded micromirror arrays.

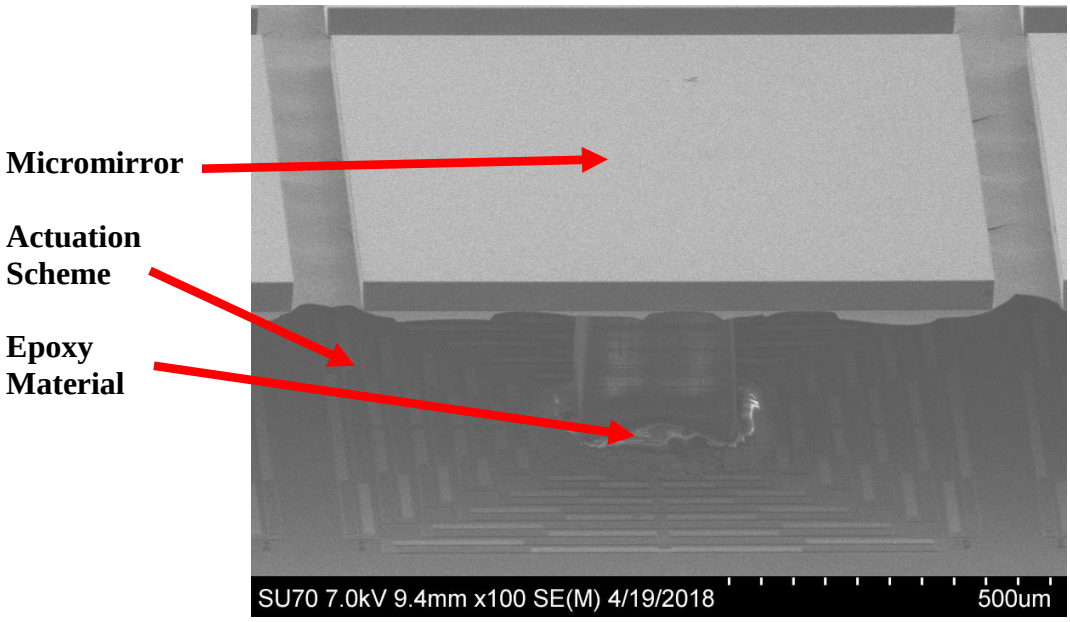

Figure 8: Image of a flip chip bonded micromirror.

This research is novel because the MEMS micromirrors being fabricated are significantly lighter than silicon micromirrors and can be grown on top of micromirror actuator arrays. Precision is critical at the micrometer scale, and it is especially important in this application since adjacent devices are only separated by 100 μm. The majority of the micromirrors will consist of SU-8; therefore, these micromirrors will be lighter than silicon based micromirrors since SU-8 is less dense than silicon.

2.5 Initial SU-8 MEMS Micromirror Design Overview

To avoid confusion, when the word *micromirror* is used it is referring to a whole structure, but without the actuation device. A micromirror in the context of this work consists of a pillar and a mirror. The pillar is the base. The mirror is held up by the pillar and is used to deflect a light source.

The pillar will be made of SU-8 photoresist. The length and width of the pillars will be 200 μm by 200 μm. The pillars' height can vary, but the goal was 25 μm. Each mirror will

consist of SU-8 sandwiched between two gold layers. It is important to note that the whole micromirror should be fully encapsulated with gold, or a metal, to keep the photoresist from deteriorating with time and create a path from the top to the base for heat dissipation. The thickness of each layer will be determined through this research; however, the length and width of the mirror will be 1 mm by 1 mm.

3. Methodology

The sections that follow will cover the initial methodology used to design, fabricate, and test MEMS micromirrors. In addition, the experimental set up that was used to find statistically significant factors will also be explained. This research is looking to replace silicon micromirrors that are currently being used in micromirror actuator arrays built and tested by AFRL and AFIT researchers [3].

It is important to note that the initial design was not used to fabricate the final structures; however, it is essential to comprehend the original design since some of the same masks are used in the final design. In addition, each different approach builds from the initial design. This chapter will only discuss the initial design, and chapter four will explain how the fabrication process evolved to a double layer design. The method of gathering data and analyzing it do not change.

3.1 Design

One of the goals of this research was to create a design that can easily be replicated in the clean room. Fabrication is somewhat of an art; therefore, simplification of the design was key to assure a trivial fabrication process. It was also important to apply an appropriate experimental design that would find the optimal material and layer thicknesses. The first step was to illustrate cross sections, create a fabrication process follower, choose an experimental design, and finally create masks.

3.1.1 Cross Sections

The illustration of cross sections was an important first step since it allows one to visually see the fabrication process. This helps one catch potential issues and makes it easy to share work that can lead to constructive criticism. The cross sections of the micromirrors that follow are

made up of only SU-8 and gold. The pillar and middle layer of the mirror consists of SU-8, and the top and bottom layer of the mirror are gold. With modifications, the same process can be used to replace the middle SU-8 layer of the mirror with SiO_2.

The fabrication process that is explained in this paragraph can be seen in Figure 9. The first mask was used to pattern alignment marks. The second mask was used to create the pillars of the micromirror. It is important to note that the SU-8 over the alignment marks was exposed to prevent an early release in the steps that follow. The third mask was used to pattern S1818. The purpose of this step was to visibly reopen the alignment marks via metal liftoff. If this step was not done, then alignment marks will not be visible for future mask alignments. The fourth mask was used to create the middle layer of the mirror. The same mask that was used in Figure 9 (c) is used again in Figure 9 (e). The final mask was used to pattern the metal layers via metal wet etch. The last step shows the release of the micromirrors. The detailed fabrication process follower can be seen in Appendix A, and the masks used in the fabrication can be seen in Appendix B.

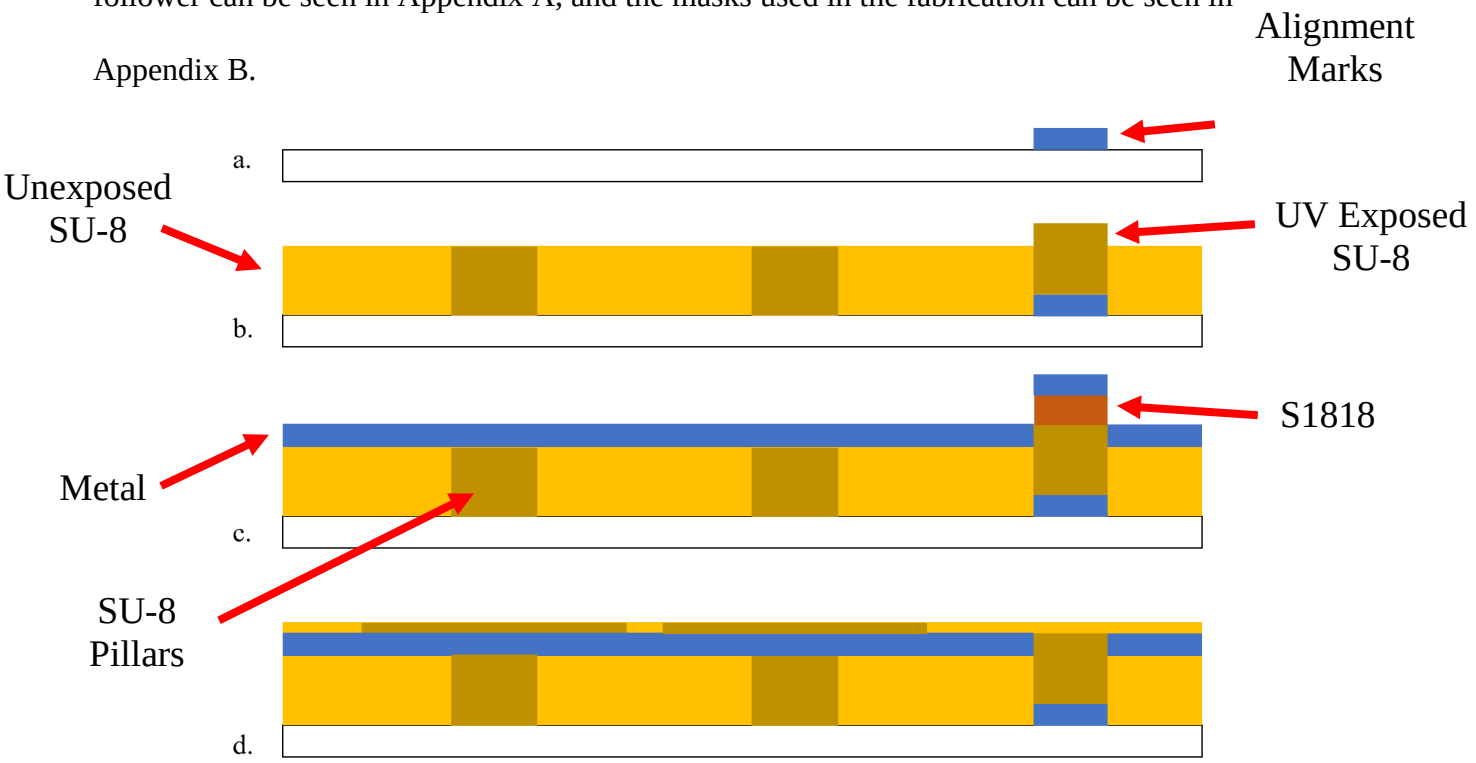

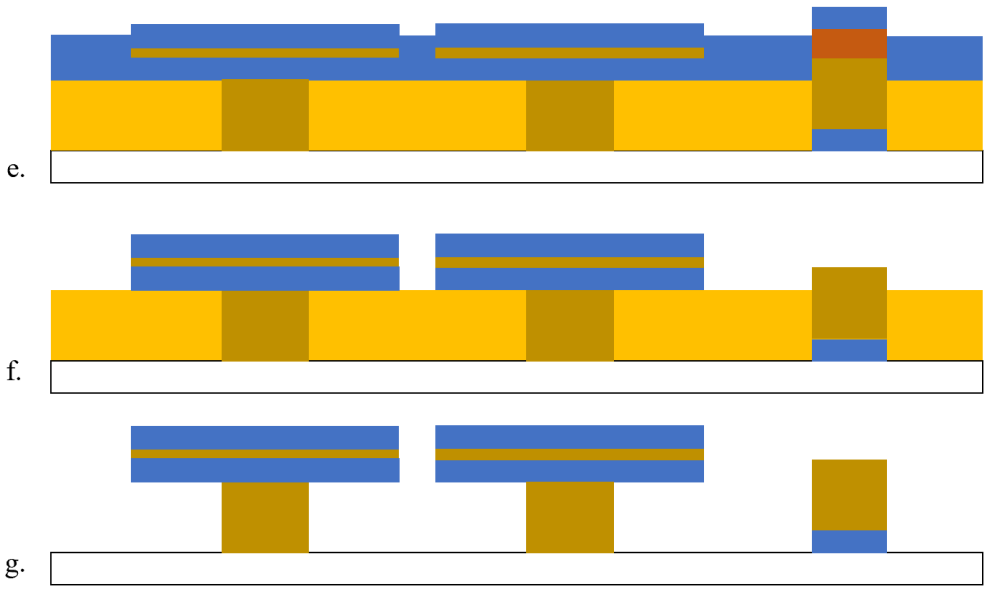

Figure 9: Alignment marks are patterned (a), pillars are created/exposed (b), S1818 is patterned and gold is evaporated (c), and middle mirror layer is created/exposed (d), S1818 is patterned and gold is evaporated (e), metal wet etch of mirror (f), and release (g).

3.1.2 Fabrication Process Follower

The fabrication process follower is one of the most important documents when dealing with any type of fabrication. This document allows one to map out the whole process step by step and helps to catch any potential mistakes. In addition, it allows one to back track and analyze a step if a mistake is encountered in the clean room. The fabrication process follower for this initial design can be seen in Appendix A.

The first potential issue dealt with the use of two different photoresists. It was unclear whether exposed or unexposed SU-8 would be affected by S1818 developer. If this was the case, then a different masking photoresist whose developer did not react with SU-8 would need to be used. Fortunately, this was not the case and the use of S1818 developer with SU-8 did not create any problems. The other potential issue dealt with an early release. This issue would be encountered after the substrate was cleaned following a metal liftoff. It was found that a standard solvent clean does not affect exposed SU-8. It is also important to note that unexposed SU-8

becomes vulnerable to a solvent clean after it has been reheated longer than the data sheet recommends. The initial process follower took extra steps to ensure this did not affect fabrication.

3.2 Experimental Design

A 2^k factorial design was used in this research. This experimental design is the most time effective and can appropriately analyze each factor. In addition, this type of design is widely used in research because the results can lead to other designs of considerable practical value [16].

3.2.1 The 2^k Factorial Design

The 2^k factorial design is commonly used in research work because its analysis investigates the joint effect of the factors on a response. As previously stated, it too forms the basis of other designs that can further explore the effects of specific factors on a response. The number of factors in the design are represented by k. Each factor has only two levels, high and low, and is represented by 1 and -1, respectively. The levels can either be quantitative or qualitative. In this case, the thickness of a layer will be quantitative and the use of either SU-8 or SiO_2 will be qualitative. This type of design provides the least number of runs with k factors that can be studied in a complete factorial design. As a result, this makes the 2^k factorial design time effective and a desired initial experimental design where many factors are being investigated [16].

3.2.2 2^4 Factorial Design

This initial research was represented by a 2^4 factorial design. The factors were the following: pillar geometry, middle mirror layer material, middle mirror layer thickness, and bottom and upper mirror thickness. The pillar geometries were a rectangle and a cylinder; however, the dimensions did remain constant. The pillar was $25\ \mu m$ high and covers as much

space as possible on the $200\ \mu m\ x\ 200\ \mu m$ surface. The middle mirror layers were SU-8 or SiO_2. The middle mirror layer thicknesses were $250\ nm$ or $2\ \mu m$. The bottom and upper mirror gold layer thicknesses were $300\ nm$ and $75\ nm$. All mirrors had an x and y dimension of $1\ mm$ by $1\ mm$. It does not matter whether qualitative factors were represented by -1 or 1; however, all smaller numerical values for quantitative factors were represented by -1 and all greater numerical values were represented by 1. Different measurements taken from the top of a given mirror were the responses of the design. All data was statistically analyzed via the statistical software Minitab 17. Appendix C shows the randomized runs that were obtained via Minitab 17 and provides further detail.

3.4 Micromirror Testing

The flatness of each micromirror was found by using the ZYGO® NewView™ 7300 Interferometer that is in the AFIT characterization lab. The interferometer was the optimal machine for this task since it can measure surface deflection and provide a topographical measurement of the entire micromirror [3].

4. Results and Analysis

The sections that follow will cover fabrication results that start from the initial design explained in Chapter 3. This chapter will show each step of the way and the reasoning behind each new fabrication run. The final fabrication design of the MEMS micromirrors consist of two layers that requires three masks to fabricate.

4.1 Initial Design

Even though extra steps are taken to guarantee that everything goes as smooth as possible in the clean room it can sometimes be difficult to predict what will happen until it is tried. Overall, the first fabrication is the toughest and most time consuming.

4.1.1 Initial Design Results

One of the first problems that was encountered dealt with having S1818 spun on top of SU-8 and can be seen in Figure 10. S1818 is used for a metal liftoff to reopen the alignment marks on the wafer. This means that all the S1818 on the wafer needs to be removed except for what is on top of the alignment marks. At first it seemed as if S1818 was not adhering to the top of SU-8. It is hard to tell since both materials are photoresists. Typically, it is easier to notice a change when the bottom layer is a metal. Another issue regarding S1818 and SU-8 had to do with the exposure dose. When S1818 is on top of SU-8, just the perfect exposure dosage needs to be used that will only pattern S1818 and not SU-8. If the S1818 is overexposed, then the SU-8 underneath it will harden and create issues in the final structure and release. To avoid this a characterization run was executed, and it was found that for a 2 μm S1818 layer an exposure dosage of 30 mJ/cm^2 is needed. An exposure dosage of 370 mJ/cm^2 was used for the pillars.

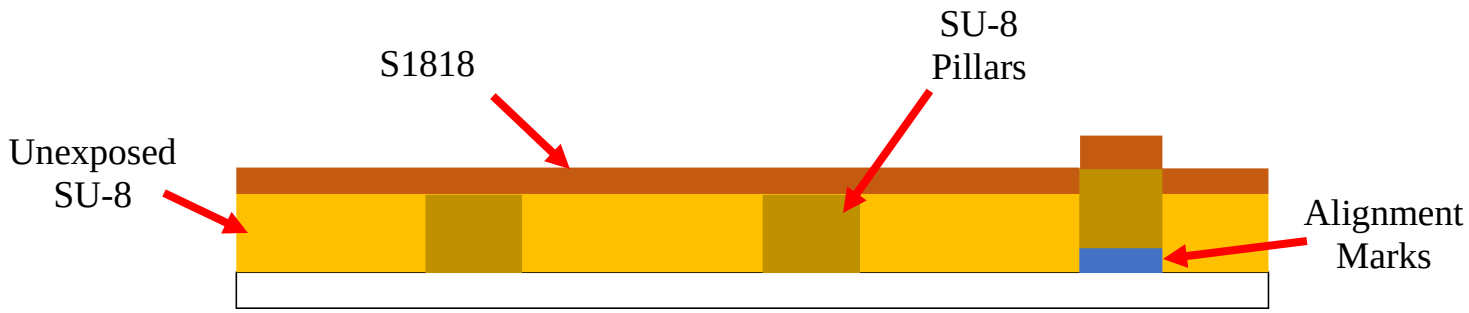

Figure 10: S1818 masking layer for SU-8.

After the SU-8 pillars have been exposed and a layer S1818 has been spun on, the next step is to use Mask C to pattern S1818 over the alignment marks for a metal liftoff after a metal evaporation. Since it was difficult to see whether S1818 was adhering on top of SU-8 and one of the goals of this research is to simplify the fabrication, one wafer with S1818 and a second wafer without S1818 were sent for metal evaporation. A metal liftoff was attempted on the wafer that did have S1818 patterned on top of it and it was observed that it did not have a clean liftoff. This might have occurred because S1818 did not properly adhere to SU-8. In addition, after the attempted liftoff the alignment marks were difficult to see under the microscope, which would result in alignment difficulties if integrated into the complete mirror fabrication process. The alignment marks were perfectly visible on the second wafer that did not have S1818 on top of it. Both the SU-8 and metal layer maintained the shape of the alignment marks.

The middle 250 nm SU-8 2002 mirror layer was to be made by diluting SU-8 2002 with 2.5 equivalents of methanol. The diluted product did not look like one consistent photoresist material. One could see that there was chunks of photoresist in the mixed product. As a result, the spin speeds of SU-8 2002 were plotted on a line and used to solve for a thickness of 250 nm. A spin speed of 6,500 rpm yields a 250 nm layer.

4.1.2 Initial Design Release

The first wafer to be released had a 250 nm SU-8 2002 middle mirror layer thickness and a 300 nm gold layer on both the top and bottom mirror layers. Figure 11 is an image of the wafer

after a metal wet etch of the top and bottom gold layers. One can see that the mirror is not flat, but the surface of the pillar is. The grooves that are seen were present after the first metal evaporation and remained through the rest of the fabrication.

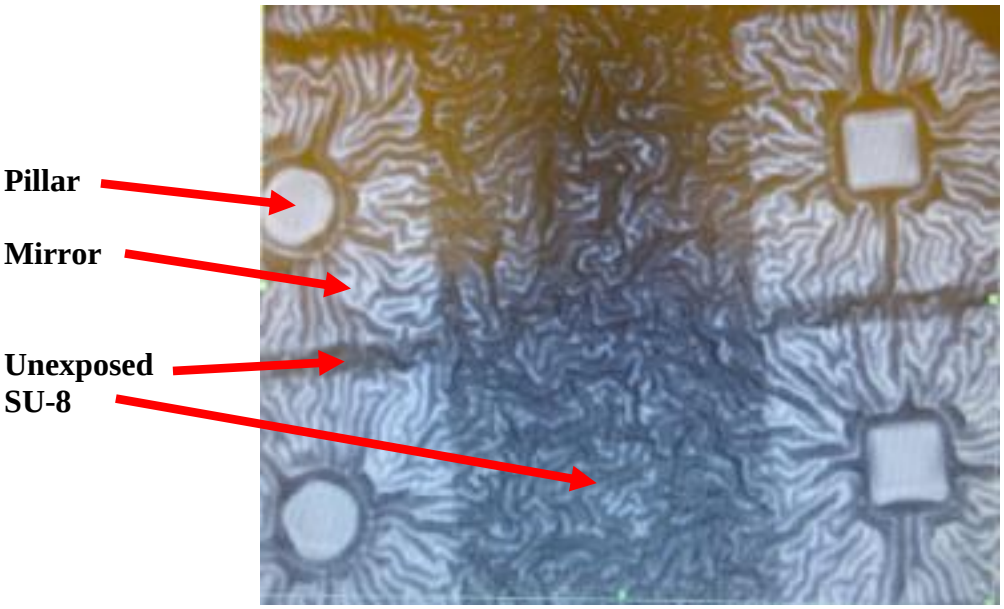

Figure 11: Micromirrors ready for release.

Different approaches were taken, but the wafer did not release. At first the wafer was submerged in SU-8 developer for 7 minutes, which is the recommended time for a 25 μm thickness. The SU-8 developer did not remove the unexposed SU-8. There was no change in the wafer. In order to attempt different release processes the wafer was diced into several pieces. Different release strategies included heating the SU-8 developer to 120^oC and 170^oC and submerging a piece in the solution for up to 20 minutes. Again, this approach did not work as there was no change in the structures. 1165 solution was also used at temperatures $65^oC, 75^oC, 95^oC, 110^oC,$ and 120^oC. At high temperatures the solution cleaned the whole wafer and at lower temperatures the solution began to remove the middle and top layer of the mirror. A mix of the two solutions was also tried and the results were the same as when only

1165 solution was used. 1165 solution is a very strong solvent that is usually used to strip wafers; therefore, any combination using 1165 solution will have the same result.

4.2 Modifications of the Initial Design

In the initial design, after the pillars were exposed a PEB was not done. This was not done because the wafer was going to be reheated in other steps; however, not doing a PEB might have contributed to a non-releasable wafer. Other ideas to potentially fabricate releasable micromirrors, were to use different SU-8 photoresists that have less viscosity than SU-8 2025. In addition, measuring the flatness of the mirror with and without a PEB was good data to have to see the effects of a PEB.

At first SU-8 2002 was substituted for SU-8 2025 to fabricate the pillars since it has the lowest viscosity among all the SU-8 photoresists. Nine layers, 3 μm each, were spun on a wafer. A full soft bake was done between each layer. After development, the profilometer measured a 2.5 μm thickness for all nine layers. This means that the layers did not adhere to one another.

SU-8 2005 was used instead of SU-8 2002 because it has the second to least viscosity among all the SU-8 photoresists. Spinning on multiple layers adhered to each other. Spinning on one and two layers at 775 rpm yielded a total thickness of 17 μm and 37 μm, respectively. To find whether a PEB was affecting the flatness of the mirror, surface measurements were taken from the unexposed to exposed pillar features. Table 1 shows the measurements taken before and after a PEB. A step height was found in both measurements after the PEB. As seen from Table 1, it is preferred not to do a PEB before the first metal bottom mirror layer deposition since each subsequent layer should maintain the same flat surface profile. In addition, a thicker layer will yield a larger step height once a PEB is done. Previous attempts to deposit metal through evaporation resulted in a non-flat surface profile, therefore sputtering was attempted.

Table 1: Step height measurements to pillar.

Thickness (μm)	**Before PEB (μm)**	**After PEB (μm)**
17	0	0.5
37	0	1.5

4.2.1 Sputtering vs Evaporation

In the initial design, the first layer of gold evaporation did not maintain a flat surface over the unexposed SU-8 (even without a PEB). In hopes of having a flat surface sputtering was attempted.

Four wafers, each with an SU-8 2005 thickness of 37 μm, had gold sputtered on them. Two of the four wafers did not undergo a PEB, and the remaining two wafers did go through a PEB. 75 nm and 300 nm are the two gold thicknesses that were sputtered on each kind of wafer (PEB vs no PEB). Figure 12 (a) and (b) are images of the two wafers that did undergo a PEB with metal thicknesses of 75 nm and 300 nm, respectively. Figures 12 (c) and (d) are images of the two wafers that did not go through a PEB with metal thicknesses of 75 nm and 300 nm, respectively. One can see that there is no major difference between all four wafers. All four wafers show grooves where SU-8 has not been exposed; however, in all four wafers the metal on top of the pillars surface is flat and conformal.

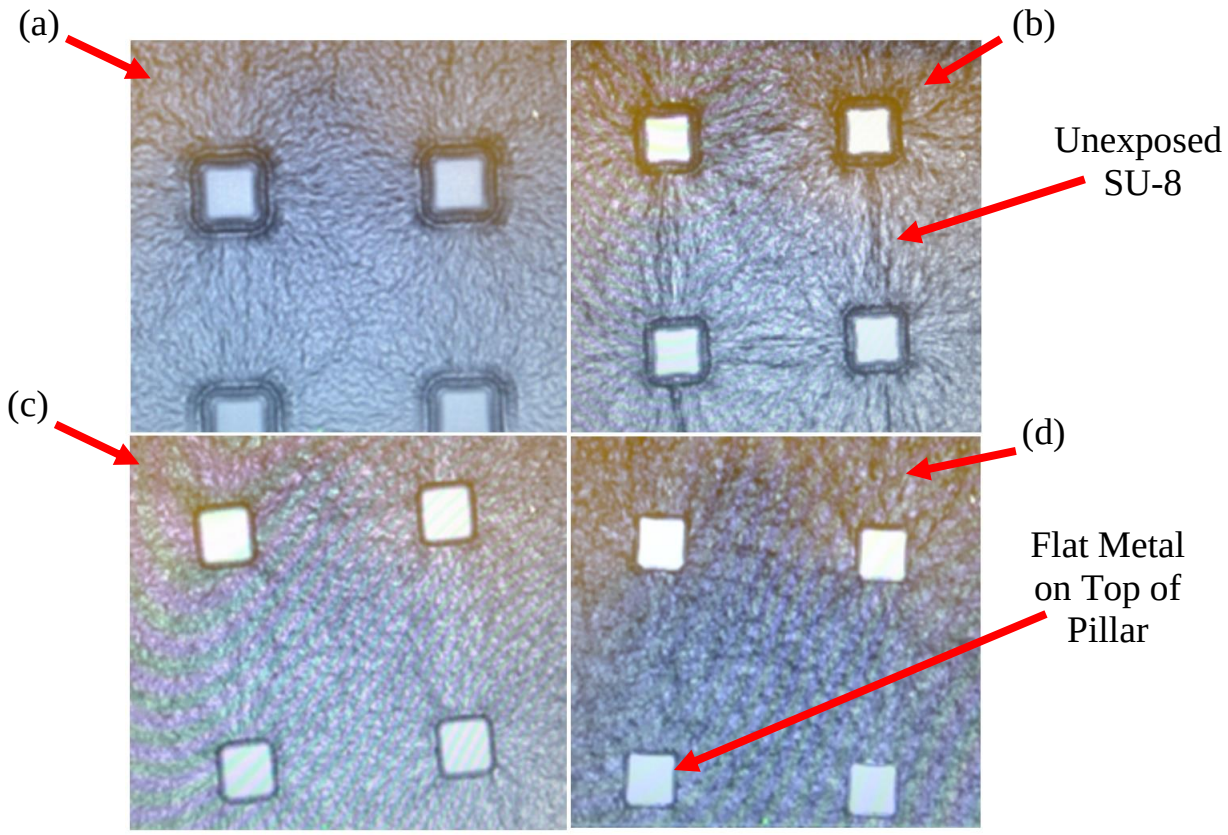

Figure 12: PEB with a gold thickness of 75 *nm* (a), PEB with a gold thickness of 300 *nm* (b), no PEB with a gold thickness of 75 *nm* (c), no PEB with a gold thickness of 300 *nm* (d).

4.3 Single SU-8 Layer Design

The initial design, or any modifications to it, did not show promise for a final micromirror with a flat surface. One thing that remained constant in the initial design was a flat metal surface over the SU-8 areas that are exposed to UV light. As a result, it is desired to have the 1 *mm* by 1 *mm* mirror part of the micromirror exposed to UV light before a metal deposition to guarantee a flat metal surface. A pillar and mirror can be fabricated with one layer of SU-8, two different exposure doses, and two masks. The process is shown in Figure 13. By varying the exposure, a micromirror structure can be made. To avoid confusion, the first exposure seen in Figure 13 (a) is going to be referred to as the mirror exposure dose (MED). The second exposure seen in Figure 13 (b) is going to be referred to as the pillar exposure dose (PED).

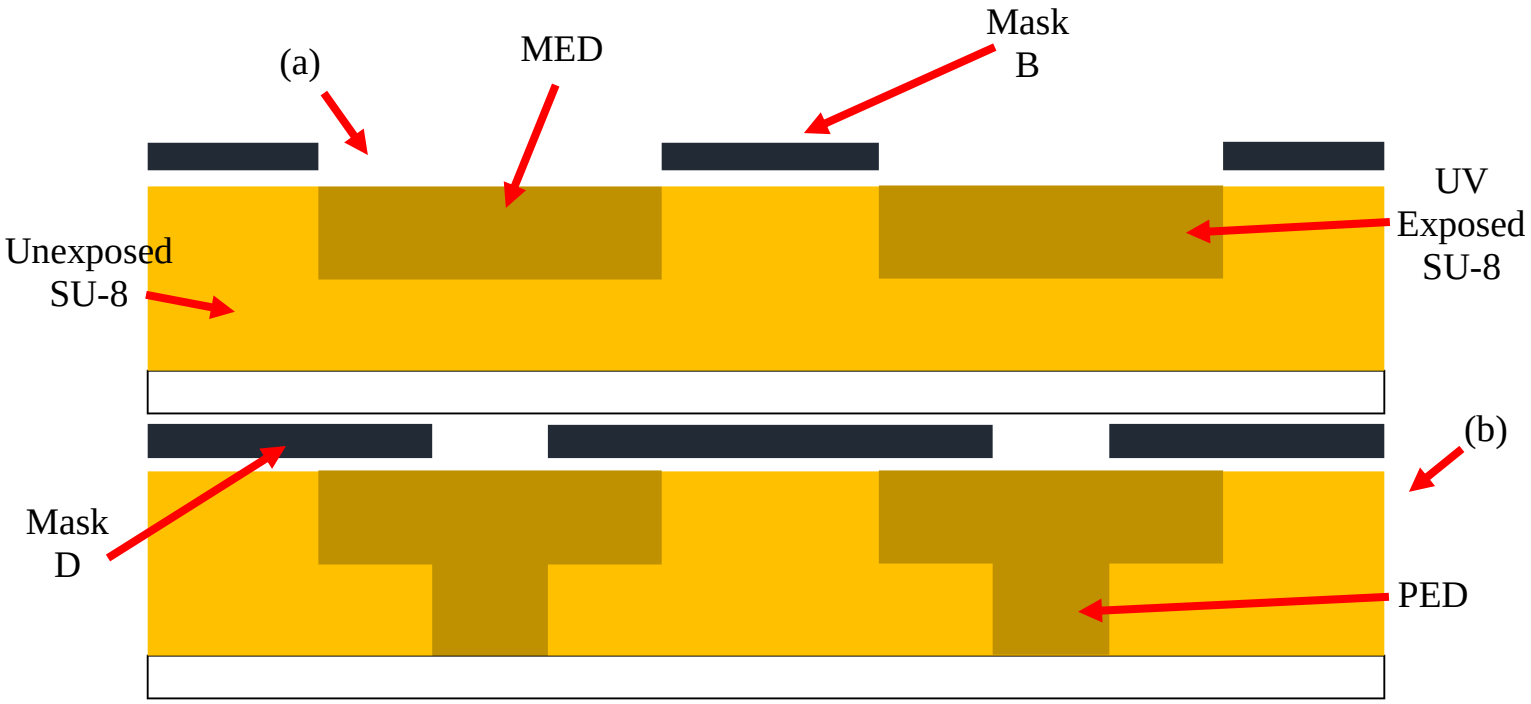

Figure 13: Dual exposure of mirror structures where the first UV light exposure, referred to as MED, is done using Mask B (a), and second pillar UV light exposure, referred to as PED, is done using Mask D (b).

4.3.1 Single SU-8 2025 Layer Characterizations

Four wafers coated with SU-8 2025 were used to test the single layer approach. The wafer with a thickness of 28 μm received a 30 mJ/cm^2 MED. The last three wafers, each with a thickness of 74 μm, received a 15, 30, and 60 mJ/cm^2 MEDs. Following each respective MED, all wafers received a 370 mJ/cm^2 PED and the appropriate PEB. Figure 14 (a) is an image of the 60 mJ/cm^2 MED wafer after the appropriate PEB, and Figure 14 (b) is an image of the 15 mJ/cm^2 MED wafer after the appropriate PEB. In Figure 14 (b) the pillar, from above, is clearly visible, and in Figure 14 (a) the pillar is not visible. This is because as the MED increases the thickness of mirror increases too. The thicker the mirror the more heat it can withstand during the PEB and not lose its surface integrity.

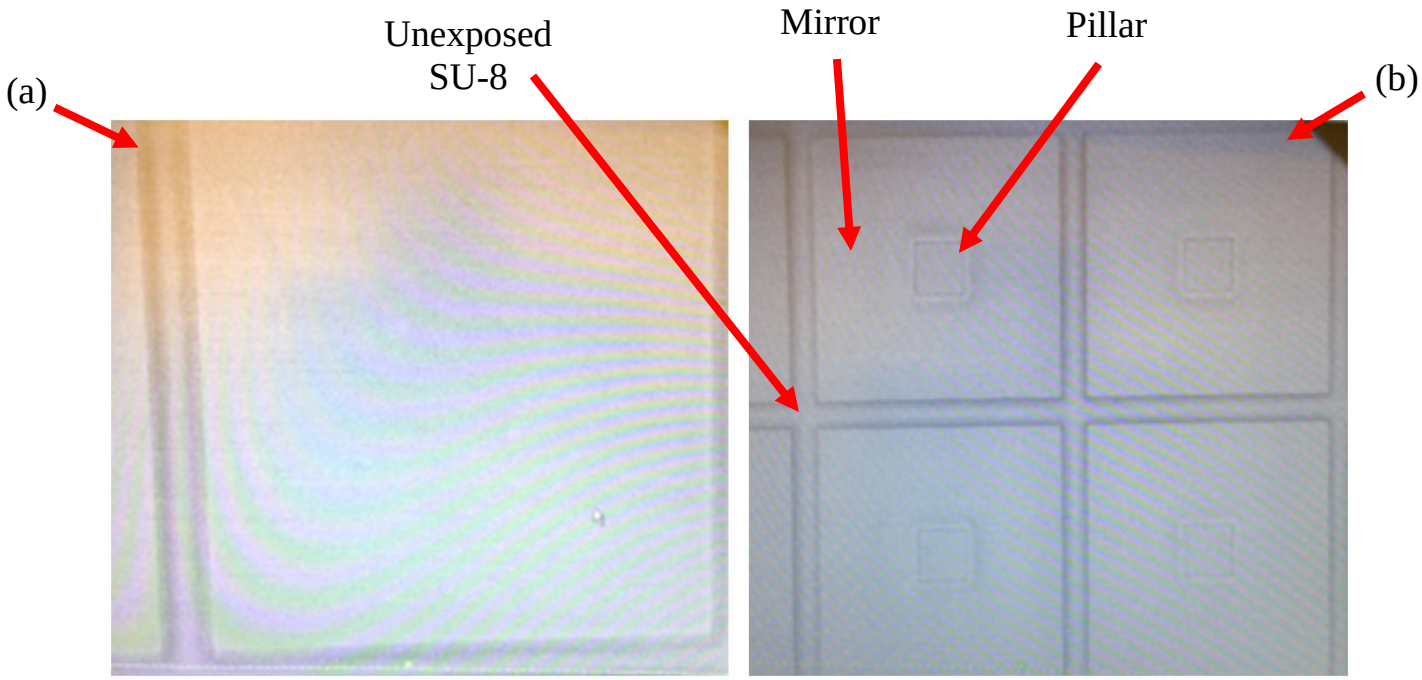

Figure 14: 60 mJ/cm^2 MED after the appropriate PEB (a), and 15 mJ/cm^2 MED wafer after the appropriate PEB.

When the wafers were submerged in SU-8 developer they did not seem to begin releasing, except for the wafer with a 15 mJ/cm^2 MED. Putting the wafers in petri dishes filled with SU-8 developer over a water sonic bath released the structures. Figure 15 shows images of the 60 mJ/cm^2 MED wafer throughout the release process. Figure 15 (a) shows the micromirror beginning to release and Figure 15 (c) is an image of the released wafer. This wafer took about 3 hours to release in the sonic bath. After the wafers were taken out of the sonic bath they were cleaned with acetone and water. Using a profilometer, a mirror thickness of 65 μm was measured from the 60 mJ/cm^2 MED wafer. A ratio of 1.083 $\mu m/(\frac{mJ}{cm^2})$ was found. This ratio proves that the greater the MED the thicker the layer. Figure 16 (a) and (b) show how the 15 and 30 mJ/cm^2 MED thin layers curled after release, respectively. Curling occurs because the top mirror layer thicknesses for 15 and 30 mJ/cm^2 MEDs are 16.25 and 32.49 μm, respectively. Both these thicknesses are not thick enough to be ridged structures. The 60 mJ/cm^2 MED wafer had a mirror thickness of 65 μm which is thick enough not to curl. In addition, the thinner the

layer the less time it takes to release. Both 15 and 30 mJ/cm^2 MED wafers took less than 10 minutes to release because the mirror is fragile. This allows developer to reach the bottom of the mirror quickly.

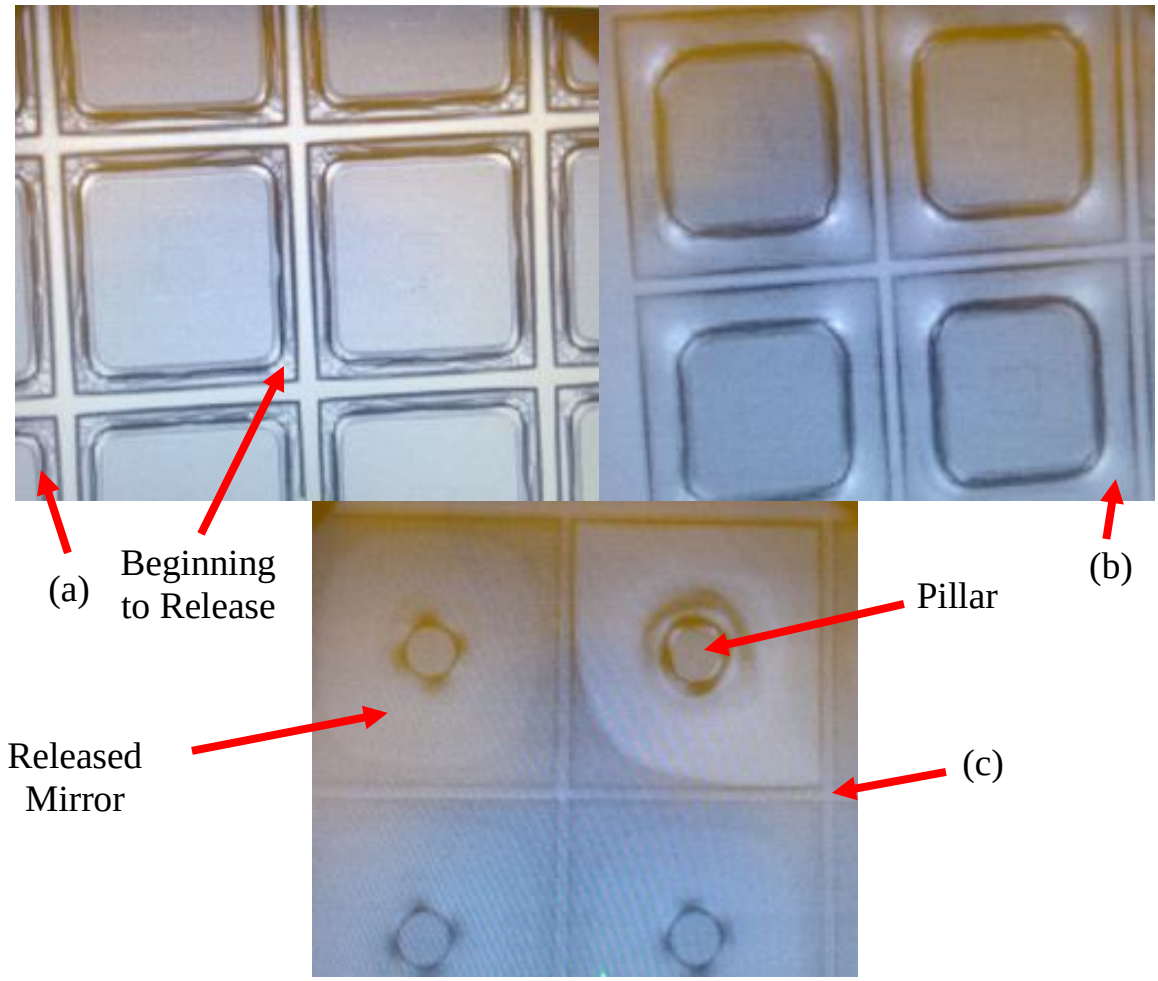

Figure 15: 60 mJ/cm^2 MED wafer releasing in sonic bath (a), 60 mJ/cm^2 MED wafer releasing in sonic bath (b), fully released 60 mJ/cm^2 MED wafer (c).

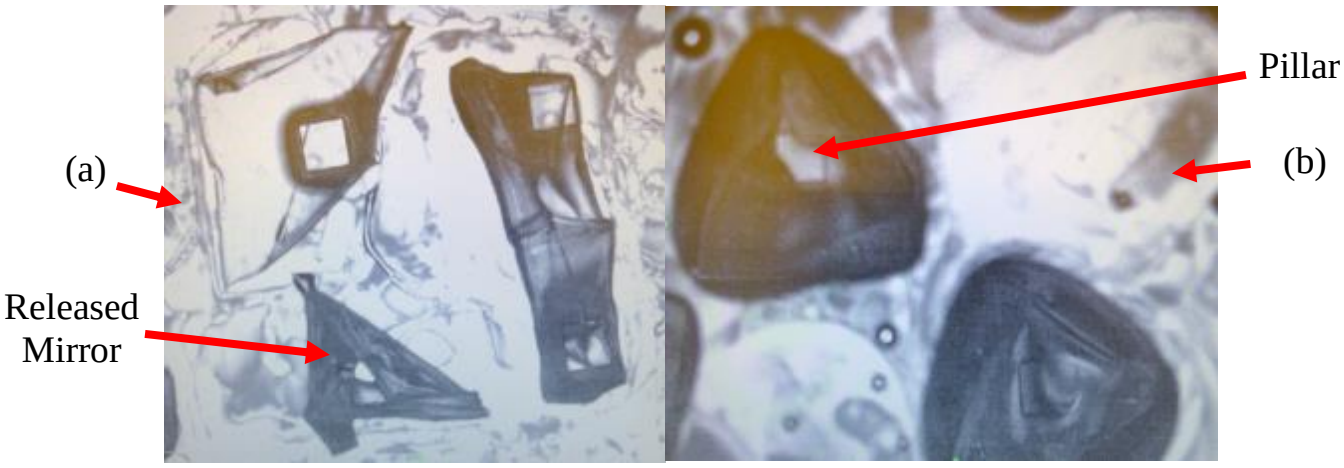

Figure 16: Fully released 15 mJ/cm^2 MED wafer (a), fully released 30 mJ/cm^2 MED wafer (b).

4.3.2 Single SU-8 2025 PED Modifications

Using the ratio found in the previous subsection and a 74 μm SU-8 2025 resist layer, it was found that a 45 mJ/cm^2 MED would yield a 25 μm pillar height and a 48.75 μm thick mirror layer. Measurements, using a profilometer, found a mirror thickness of approximately 48-49 μm which is close to the calculated value. The micromirrors released in approximately 45 minutes.

Surface measurements were taken from the mirror to the pillar, after a PEB, and approximately found a 1 μm step height. To try and avoid a step height, a PED of 80 and 75 mJ/cm^2 was used instead of 370 mJ/cm^2 to see if overexposure was the cause; however, changing the PED to a lower exposure dose did not change the 1 μm step height. Another alternative to fix this problem was to first pattern the pillars, spin on an additional layer of SU-8, and expose the mirror layer. This approach did not work because the additional resist layer maintained the integrity of the pillar creating a step height. Finally, using more than two resist layers did not work because a step height was still present as previously mentioned.

4.4 Double Layer Design: SU-8 2025 and Gold

A design, using three wafers, was conducted to see how an evaporated gold layer affected the single SU-8 layer approach. Each wafer was coated with a 74 μm SU-8 2025 layer. Wafer A, B, and C had a 43, 45, and 50 mJ/cm^2 MEDs, respectively. Table 2 summarizes other values that include: pillar height, mirror thickness, and gold thickness.

Table 2: Double layer design specs.

Wafer	MED (mJ/cm^2)	PED (mJ/cm^2)	Pillar Thickness (μm)	Mirror Thickness (μm)	Gold Thickness (nm)
A	43	370	27	47	300
B	45	370	25	49	300
C	50	370	20	54	300

Figure 17 is an image of Wafers A and B with each having a 300 nm gold layer. One can see that the mirror surface layer looks smooth. Surface profile measurements of Wafers A, B, and C can be seen in Figure 18. The dip from the pillar to the mirror for Wafers A, B, and C are 0.94, 0.15, and 0.09 μm, respectively. From these measurements it can be assumed that the surface becomes flatter as the MED increases. This is because the mirror layer is thicker for greater MEDs and allows it to maintain its surface profile.

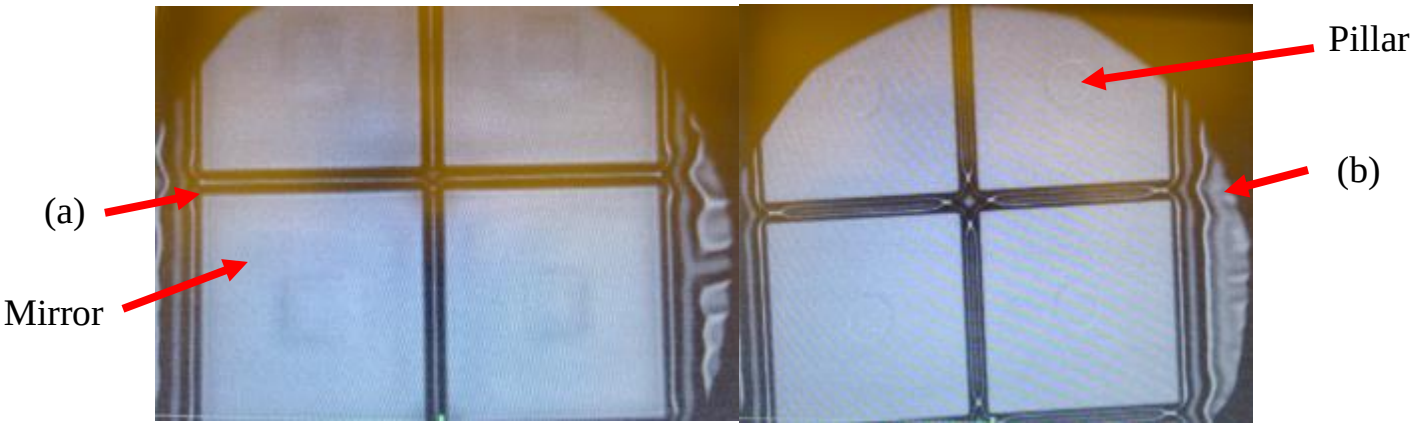

Figure 17: Wafer A with a top gold layer (a), and Wafer B with a top gold layer (b).

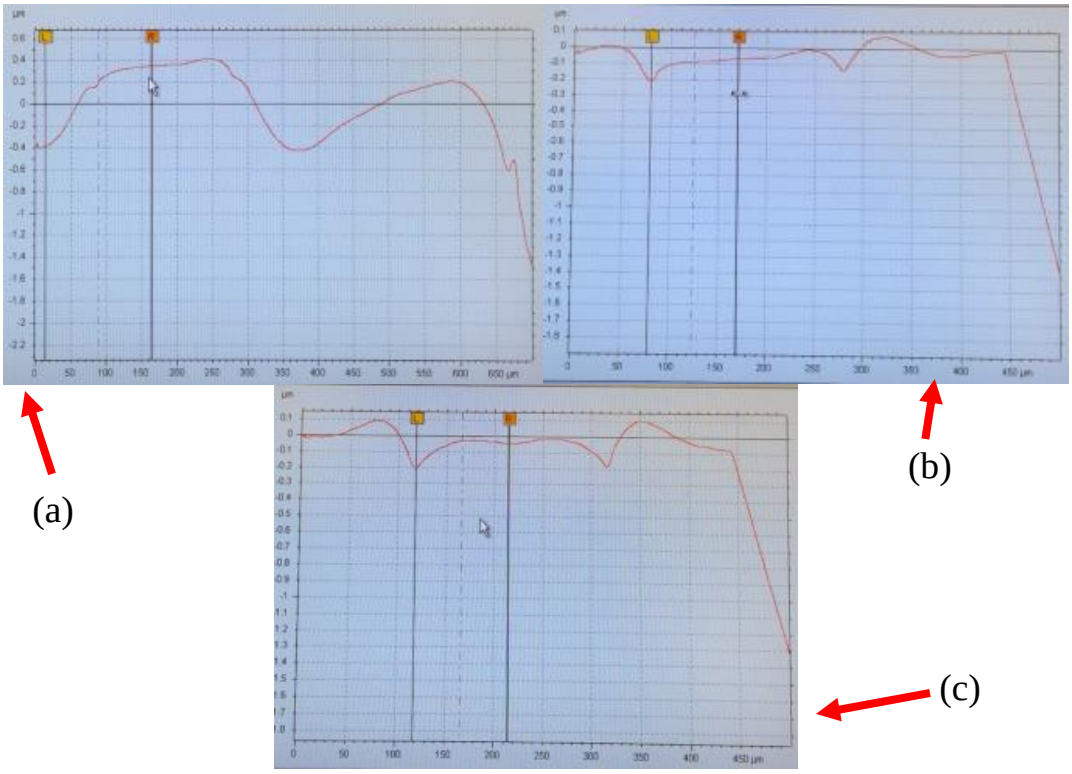

Figure 18: Wafer A surface profile (a), Wafer B surface profile (b), and Wafer C surface profile (c).

All wafers were patterned with Mask E and then a metal wet etch was done. All wafers look the same after the metal wet etch and can be seen in Figure 19. All three wafers were put in their own petri dishes containing SU-8 developer and put in a sonic bath to release. All wafers lost about one fourth of the gold mirror layer. One could see that the mirrors in Wafer A curled the most. Wafer C had the least curvature in the mirrors. In addition, Wafer A took the least time to release and Wafer C took the most time. Wafer C took about five hours to release and Wafers A and B took about 2.5 hours. An image of Wafer C can be seen in Figure 20 (a). Figure 20 (b) is an image of Wafer C after it has dried for over 12 hours. All wafers were cleaned with acetone and water following the release.

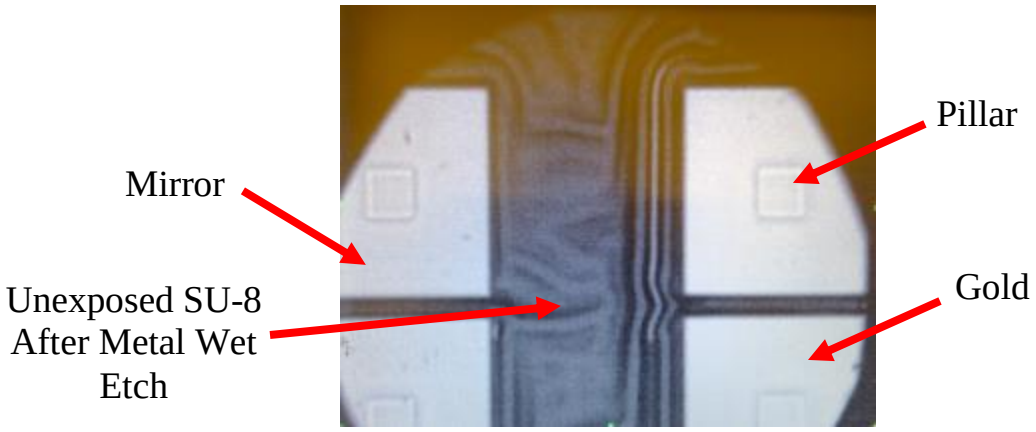

Figure 19: Post metal wet etch.

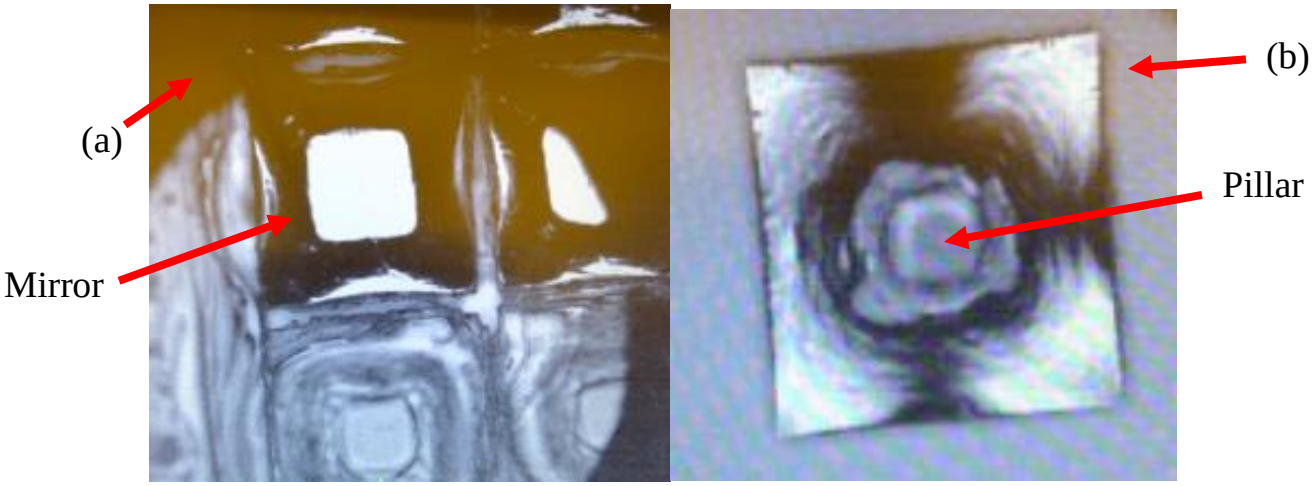

Figure 20: Wafer C after the sonic bath release (a), Wafer C after it has dried for 12 hours (b).

4.4.1 Double Layer Design: SU-8 2025 and Gold, Takeaways

The metal might have been removed from some of the mirrors due to the metal wet etch, and an adhesion layer could help this issue. The sonic vibrations could also contribute to metal falling off of mirrors during the release. In addition, the release time might decrease if a thicker layer of SU-8 is used to create more space for the solution to travel through. Finally, an SU-8 photoresist with a greater viscosity might create more ridged mirror surfaces with the same MEDs.

4.5 Single SU-8 2050 Layer Characterizations

SU-8 2050 photoresist was used next since it has a greater viscosity than SU-8 2025. A single layer spun on at 1000 rpm yields a total thickness of approximately 136-140 μm, which means that there is enough space for SU-8 developer to release the structure in a reasonable time. Various wafers were sectioned off and exposed at different MEDs. The MEDs are as follows: 10, 12, 14, 16, 18, 20, 22, 24, 30, 32, 34, 36, 38, 40, 42, 44, 45, 50, 55, 60, and 70 mJ/cm^2. Table 3 summarizes the release times, mirror to pillar step height for both squares and circles (after a PEB but before releasing), and the step height from the unexposed area to the mirror (after a PEB but before releasing). Overall all measurements increase as the MEDs increase. The surface profile seen in Figure 21 is consistent with all MEDs (N/A is short for not available).

Table 3: Specifications for various MEDs.

MED (mJ/cm^2)	**PED (mJ/cm^2)**	**Release Time (minutes)**	**Mirror to Square Pillar Step Height (μm)**	**Mirror to Circle Pillar Step Height (μm)**	**Unexposed Area to Mirror Step Height (μm)**
10	370	4	N/A	N/A	N/A
12	370	5	N/A	N/A	N/A
14	370	5	N/A	N/A	N/A
16	370	5	N/A	N/A	N/A
18	370	5	N/A	N/A	N/A
20	370	9	N/A	N/A	N/A
22	370	15	N/A	N/A	N/A
24	370	24	0.86	0.92	2.38
28	370	N/A	0.85	0.74	2.22
30	370	45	0.55	0.59	2.40
32	370	81	N/A	N/A	N/A
34	370	81	0.5	0.52	2.62
36	370	81	N/A	N/A	N/A
38	370	81	N/A	N/A	N/A
40	370	81	0.68	0.72	2.60
42	370	81	N/A	N/A	N/A
44	370	81	0.67	0.75	2.56
45	370	90	N/A	N/A	N/A
50	370	100	1.06	1.02	3.30

55	370	100	N/A	N/A	N/A
60	370	240	0.91	0.93	3.96
70	370	240	N/A	N/A	N/A

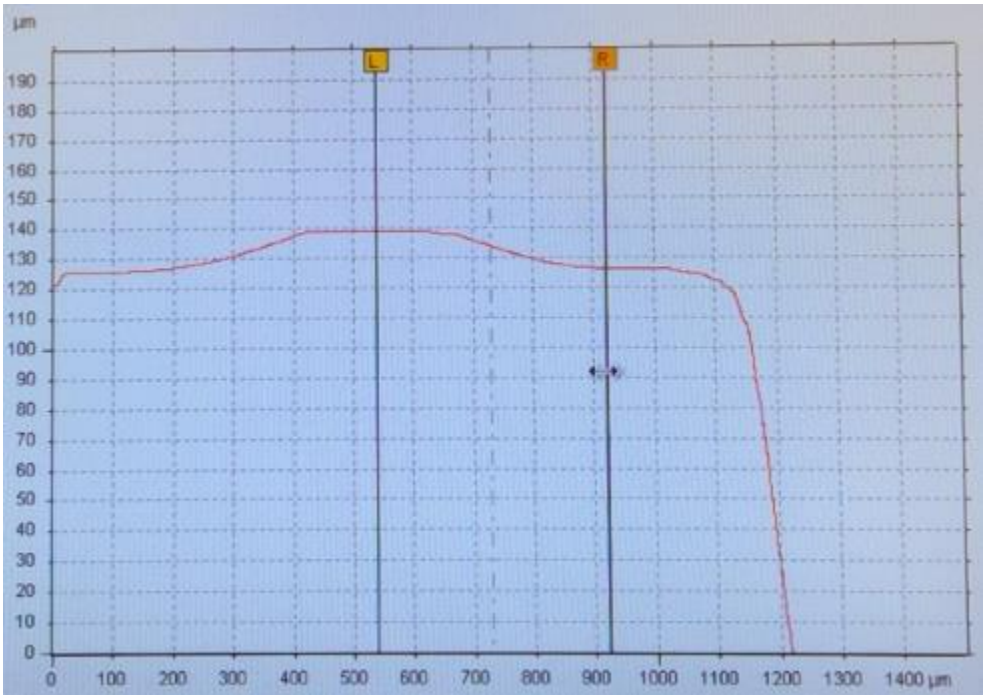

Figure 21: General surface profile after a PEB.

4.5.1 Double Layer Design: SU-8 2050 Release Followed by a Gold Deposition

The sonic bath vibrations could have caused some of the metal to fall of the mirrors. An experiment was conducted to see if releasing the structures before the metal deposition is worthwhile. Two wafers, each with a 140 μm SU-8 2050 layer, were exposed with a MED of 50 and 55 mJ/cm^2, respectively. The PED for both wafers remained at 370 mJ/cm^2. Following release and a solvent clean, both wafers had 300 nm of gold evaporated. Figure 22 is an image of the 50 mJ/cm^2 MED wafer after a metal wet etch is complete. One can see that not all the gold is gone between the mirrors since the S1818 did not uniformly spread throughout the wafer. In addition, some of the mirrors might have been attached to the substrate which made it possible for S1818 to spin on at 4000 rpm. At a spin speed of 4000 rpm one would expect some

micromirrors to fly off, but none did. As is, this method is undesirable. Possible modifications to this process are recommended in Chapter 5.

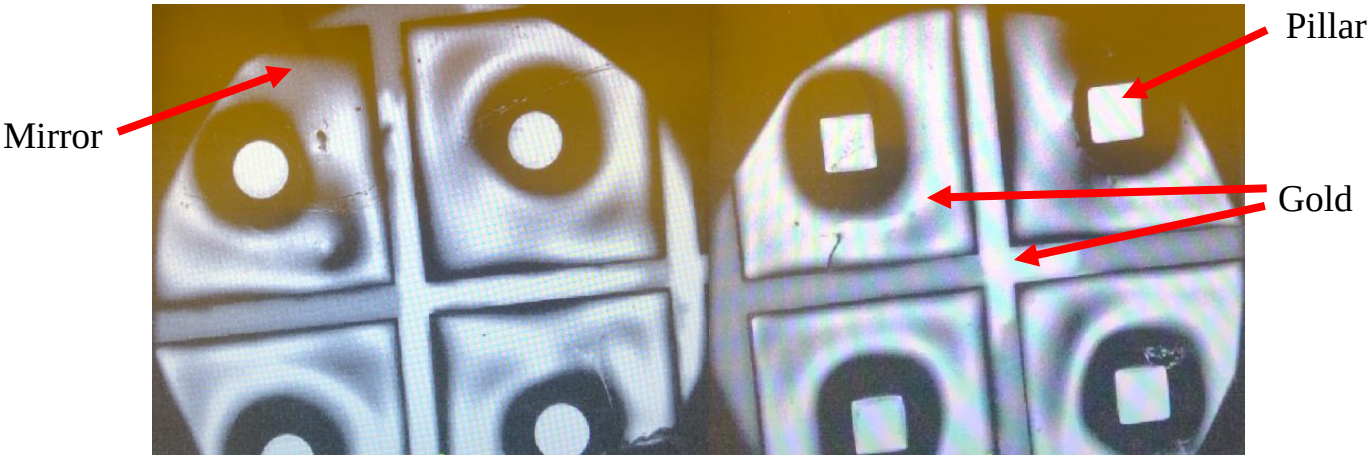

Figure 22: 50 mJ/cm^2 MED wafer after a metal wet etch is complete.

4.5.2 Double Layer Design: SU-8 2050 and Gold

For this design 8 wafers were used. Each wafer received two different MEDs, and all wafers had the same 140 μm resist layer. One MED was used in the top half of the wafer, and the other MED was used on the bottom half of the wafer. This assured that each different kind of MED, on each wafer, had both square and circle pillar geometries. The different pairs of MEDs, in mJ/cm^2, are as follows: 24 & 28, 30 & 34, 40 & 44, and 50 & 60. Each wafer pairs received two different aluminum thicknesses, 0.5 μm and 1 μm. The order of metal layers from bottom to top are as follows: chrome, aluminum, chrome, and platinum. Only the aluminum layer thickness varied between pair runs, and all depositions were done via sputtering. This experiment was trying to see whether a thick metal layer could reduce SU-8 curvature upon release and if the use of an adhesion layer maintained all the metal on the mirror.

4.5.2.1 Single Layer Liftoff via Sonic Bath

The release of the micromirrors was done via a process I am calling single layer liftoff (SLL). For all the wafers in this design, the step height from the unexposed area to the mirror is greater than 2 μm; therefore, it was expected that the metal be removed from all unexposed resist areas as unexposed resist is removed via a sonic bath. This method proved to successfully as it removed the metal from undesired areas upon release. Note that this method consists of submerging a wafer in a petri dish that is filled with SU-8 developer and placed in a water filled sonic bath. The 0.5 μm metal thick layer took approximately 15 to 21 minutes for the SLL to completely remove unwanted metal between micromirrors. An image of this can be seen in Figure 23 (a). The 1 μm metal thick layer took about 30 to 35 minutes for the SLL to finish and did not remove any of the metal on top of the mirror surface. An image of this can be seen in Figure 23 (b). The thicker the metal the less vulnerable it is to sonic bath vibrations because it is rigid. In addition, the thicker the metal the more time it will need to be removed from unwanted areas because there is sturdy.

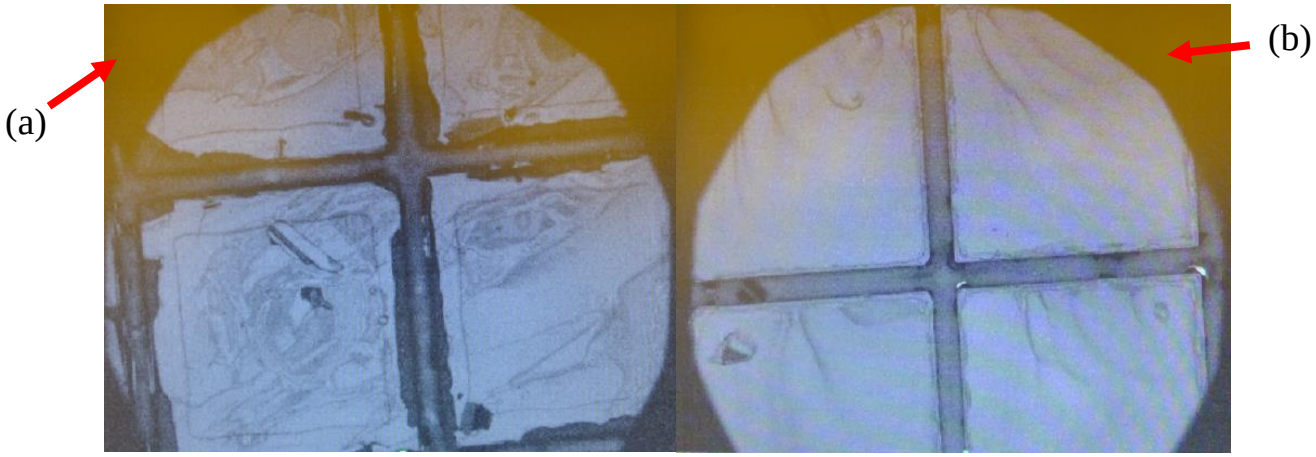

Figure 23: SLL via sonic bath for a 0.5 μm metal thickness (a), SLL via sonic bath for a 1 μm metal thickness (b).

4.5.2.1.1 SLL vs Traditional Liftoff

To see whether a common liftoff yielded better features than a SLL, two wafers were tested. Following the double exposure of the SU-8 and a PEB, a 2 μm S1818 was patterned on top of the SU-8 layer using Mask D. Then one wafer received a 0.5 μm metal layer deposition, and the other wafer received a 1 μm metal layer deposition. An acetone bath did not remove any of the unwanted metal. This led to placing the wafer in a petri dish filled with acetone into a sonic bath. Doing this destroyed the structures and wiped the whole wafer clean. The second wafer was put in a petri dish filled with SU-8 developer into a sonic bath. This as well destroyed the structures and wiped the wafer clean. The high heat required during the S1818 soft bake might be causing this issue. As well, this research has found that S1818 does not properly adhere on top of SU-8 photoresist and this factor might be contributing to this result. For this research, SLL via a sonic bath is the preferred method to remove unwanted metal.

4.5.2.2 Double Layer Design: SU-8 2050 and Gold Release via Sonic Bath Results

All wafers, except both 50 & 60 mJ/cm^2 MED wafers, were released in a water filled sonic bath using petri dishes filled with SU-8 developer. The last two wafers were saved for a later time because the released wafers were not showing promising results. The sonic vibrations created too much agitation that caused the metal layers and SU-8 mirror layer to lose its integrity during the release. Figure 24 (a) and (b) is an image of a wafer, post release, that had a 1 μm aluminum layer deposition with MEDs of 30 and 34 mJ/cm^2, respectively.

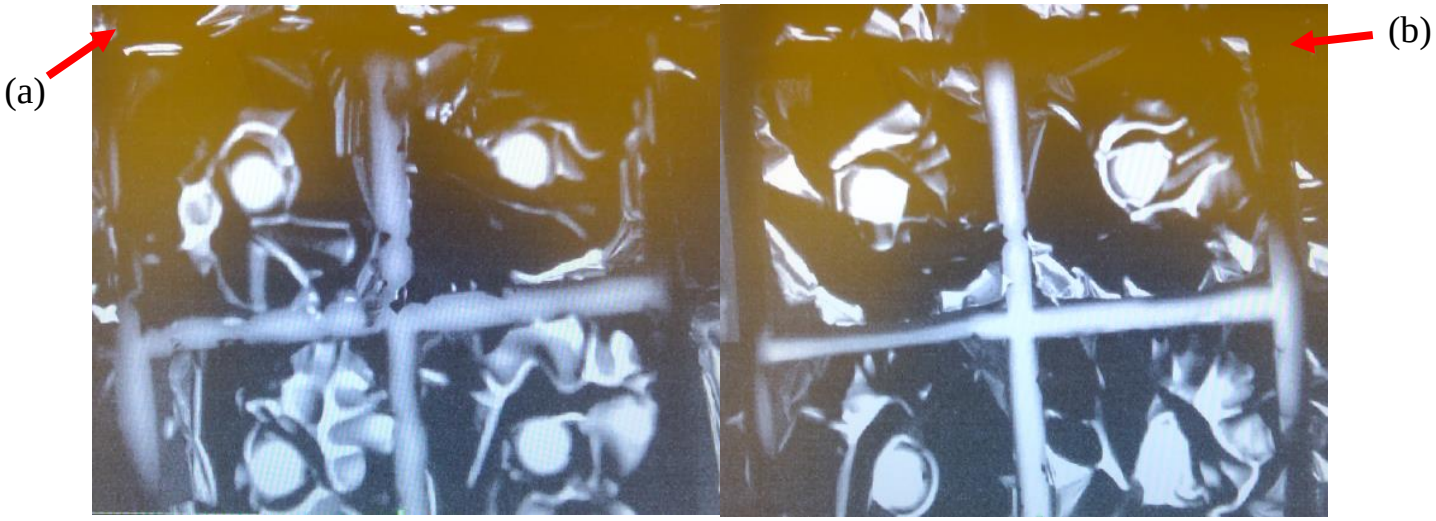

Figure 24: 1 μm aluminum layer deposition with a 30 mJ/cm^2 MED (a), 1 μm aluminum layer deposition with a 34 mJ/cm^2 MED (b).

4.6 Final Release Process via Magnetic Hotplate Spinner Characterization

A new release process was explored to avoid the agitation created by the sonic bath and can be seen in Figure 25. The new process consists of 150 mL of SU-8 developer, a 500 mL glass beaker, and a large magnetic stirrer (approximately the length of the glass beaker's diameter). The glass beaker was filled with 150 mL of SU-8 developer, then the magnetic stirrer was placed in the beaker. Finally, the wafer, patterned side up, was dropped inside the glass beaker. The magnetic hotplate spinner was set to 180 rpm. A characterization run, with a 140 μm SU-8 2050 thickness, with four different MEDs was executed. The MEDs for the characterization run were as follows: 30, 40, 50, and 60 mJ/cm^2.

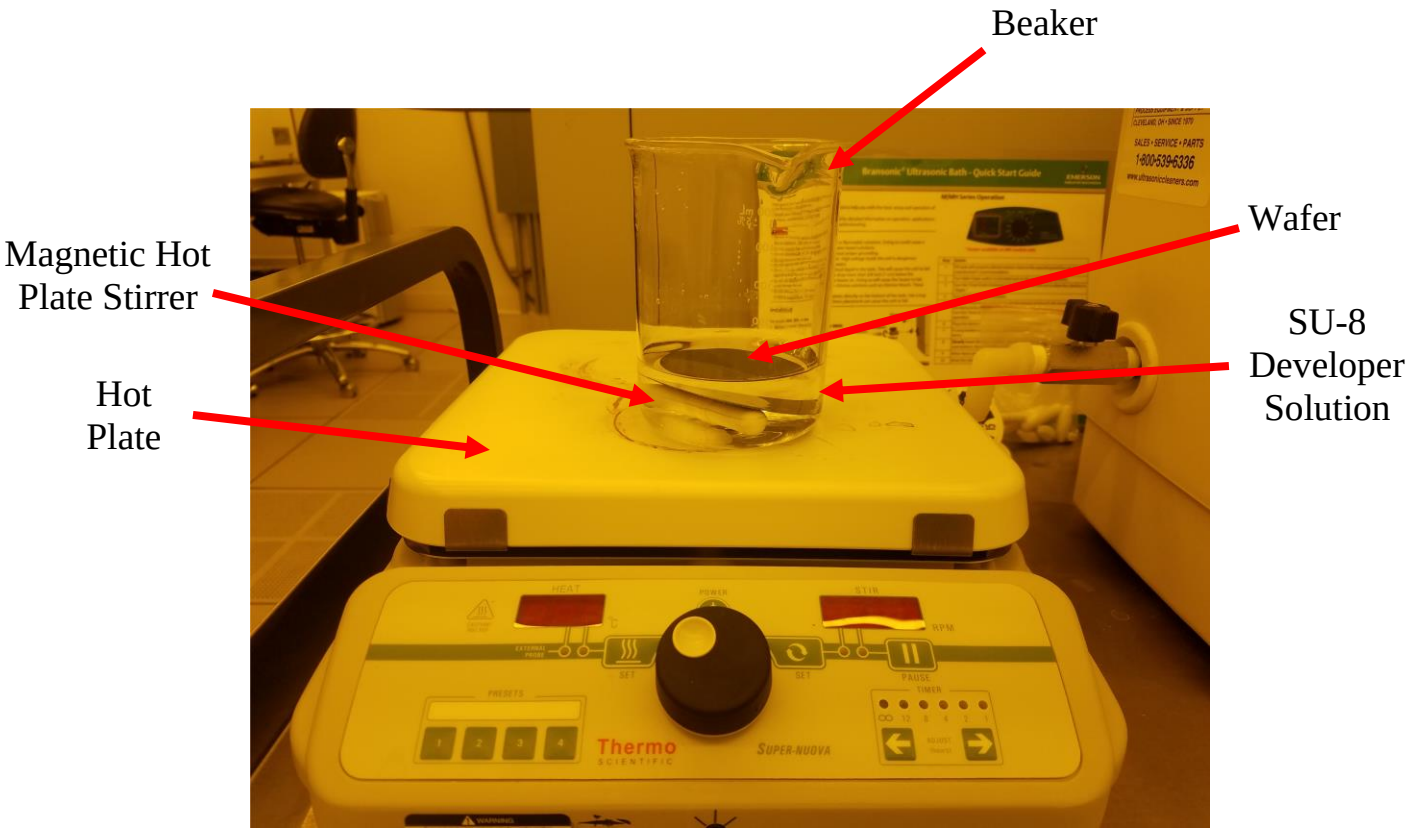

Figure 25: Magnetic hot plate spinner release set up.

Table 4 summarizes the release times. The 60 mJ/cm^2 MED was heated to 65^oC at the 140-minute mark to speed up the release time.

Table 4: Release times using a magnetic hotplate spinner.

MED (mJ/cm^2)	**PED (mJ/cm^2)**	**Release Time (minutes)**
30	370	50
40	370	90
50	370	100
60	370	160

4.7 Final Experimental Set Up

The same fabrication run used in section 4.5.2 was used in this final fabrication run; however, only 4 wafers were used opposed to 8 wafers. The other modification was that the two pairs of MEDs were 30 & 40 and 50 & 60 mJ/cm^2. The same metal thicknesses were used, and

all metal depositions were done via sputtering. These four wafers were not patterned with S1818 and instead undergo a SLL via a sonic bath to remove unwanted metal. Then each wafer is released via the magnetic hotplate stirrer process that is explained in section 4.6. Following release, each wafer is submerged in a water filled petri dish to clean any residual residue. Each wafer, balanced between two mask holders facing upside down, was left over night to dry. This helped the mirrors not stick to the wafer. The detailed fabrication process follower for this final run is included as Appendix D.

4.7.1 Final Experiment Set Up Results

The top metal layer of the two wafers that had a 0.5 μm metal layer cracked. This occurred because a metal layer thickness of 0.5 μm is too thin to withstand sonic bath vibrations. Regardless of the MED, if the metal thickness is too thin then the metal layer will crack. Both wafers with 30 & 40 mJ/cm^2 MEDs curled regardless of the metal layer thickness. Curvature is seen in these wafers because the thickness of the mirror is thin, due to a low MED, and cannot maintain its flat surface profile. This also proved that if the mirror thickness is thin, then the metal layer on top (thin or thick) will not help keep the surface flat. The only run that showed a conformal surface is the remaining wafer with a 1 μm metal layer and 50 & 60 mJ/cm^2 MEDs. These results are discussed in the section that follows.

4.7.2 Interferometric Measurements

Various 3D measurements of the surface profile were taken using the ZYGO® NewView™ 7300 Interferometer located in the AFIT characterization lab. Measurements were only recorded from the wafer with a 1 μm metal layer and 50 & 60 mJ/cm^2 MEDs. Interferometer images were taken for all wafers except those with a 0.5 μm metal layer because the metal layer on those wafers cracked. Several measurements were taken for five different

micromirror profiles. Each set of five micromirrors were picked from an array of 5 by 5. The third row of one 5 by 5 micromirror array was analyzed for both circular and rectangular pillar geometries at the two different doses. The different measurements are as follows: height difference from the center of the pillar to each four ends of the mirror, height difference from the center of the pillar to each four corners of the mirror, and the height difference from the center of the pillar to the first dip of the mirror.

Interferometer images were taken for both wafers with a 1 μm metal layer. Single and array micromirror images were taken; however, data points were not taken for all micromirrors. Data points for 30 & 40 mJ/cm^2 MEDs could not be measured because the interferometer needs a somewhat flat surface to analyze. Single micromirror interferometer images of 30 mJ/cm^2 MED with circular and square pillar geometries can be seen in Figure 26. One can see that there is no major change in the cross-section profile when varying the pillar geometry; therefore, there is no significant difference between both 3D surface topographies. Both micromirrors curve upward along the corners and sides of the mirror. Interferometer images showing micromirror arrays for both pillar geometries at 30 mJ/cm^2 MED can be found in Appendix E.

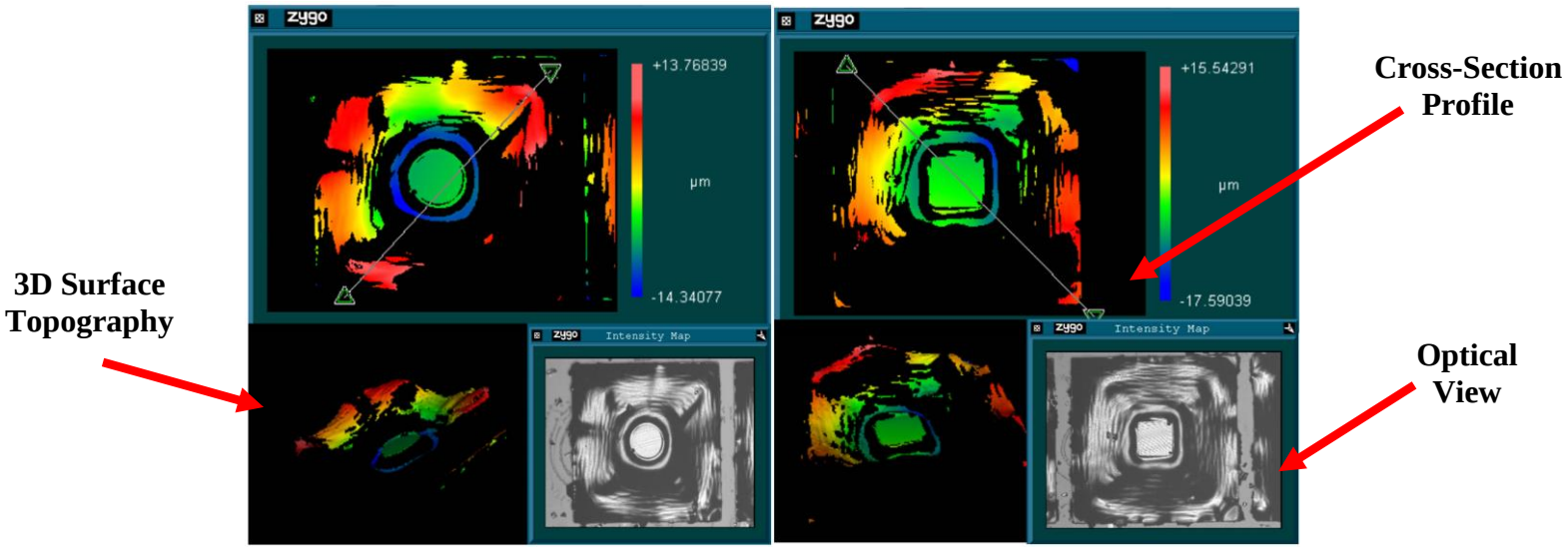

Figure 26: A single 30 mJ/cm^2 MED micromirror with a circular pillar (left), and a single 30 mJ/cm^2 MED micromirror with a square pillar (right).

The same conclusions made for the micromirrors with 30 mJ/cm^2 MED can be made for the micromirrors with 40 mJ/cm^2. There is no major difference when comparing both cross-section profiles and can be seen in Figure 27. Regardless of the pillar geometry, both micromirrors curl upward in all outer mirror directions. Interferometer images showing micromirror arrays for both pillar geometries at 40 mJ/cm^2 MED can be found in Appendix E.

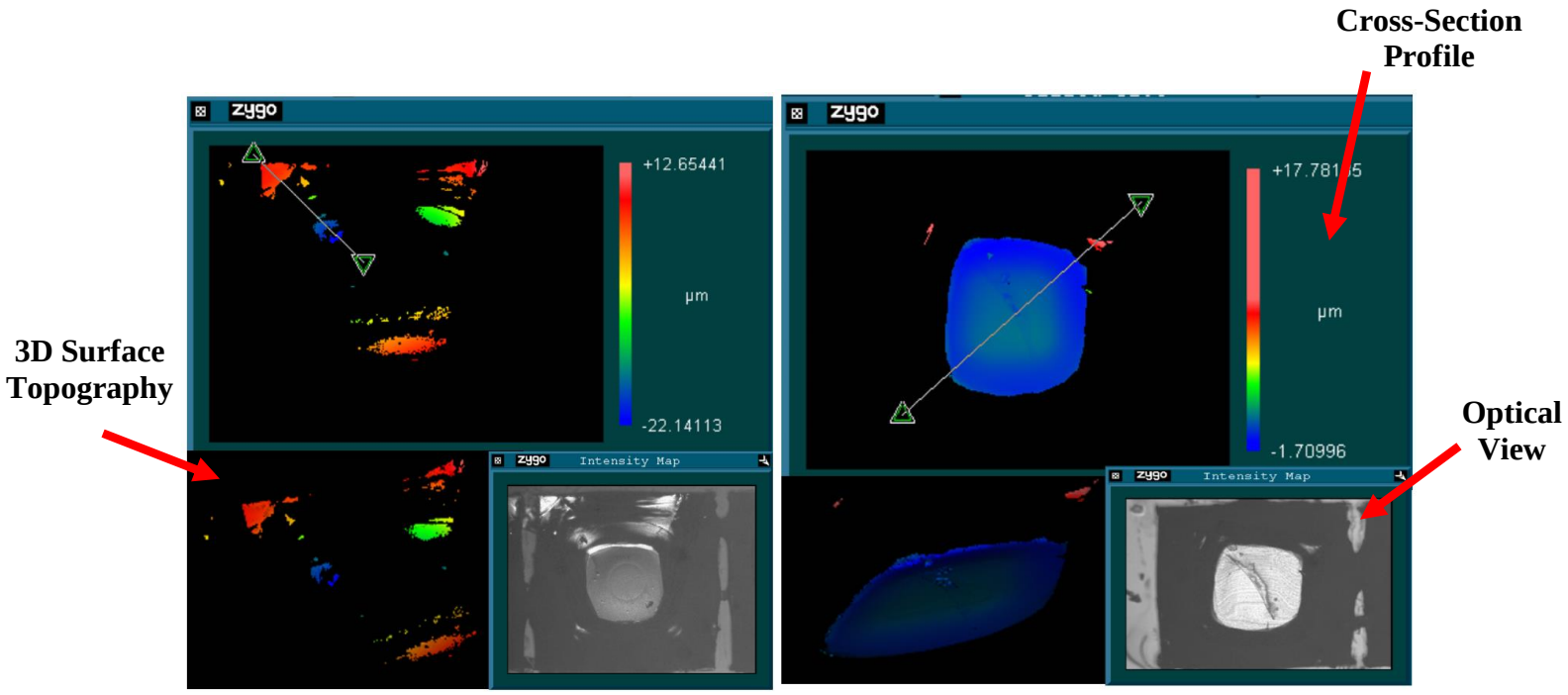

Figure 27: A single 40 mJ/cm^2 MED micromirror with a circular pillar (left), a single 40 mJ/cm^2 MED micromirror with a square pillar (right).

Figure 28 and 29 shows interferometer images of a single 50 mJ/cm^2 MED with circular and square pillar geometries, respectively. One can see that the cross-section profile for the micromirror with a square pillar geometry, seen in Figure 29, is more complete than the micromirror with a circular pillar, seen in Figure 28. A cross-section height profile can now be analyzed by the interferometer because the MED has increased from 40 to 50 mJ/cm^2. The pillar geometry is most likely affecting how the SU-8 developer travels under the mirror and in this case a square pillar is preferred over a circular one. Interferometer images showing micromirror arrays for both pillar geometries at 50 mJ/cm^2 MED can be found in Appendix E.

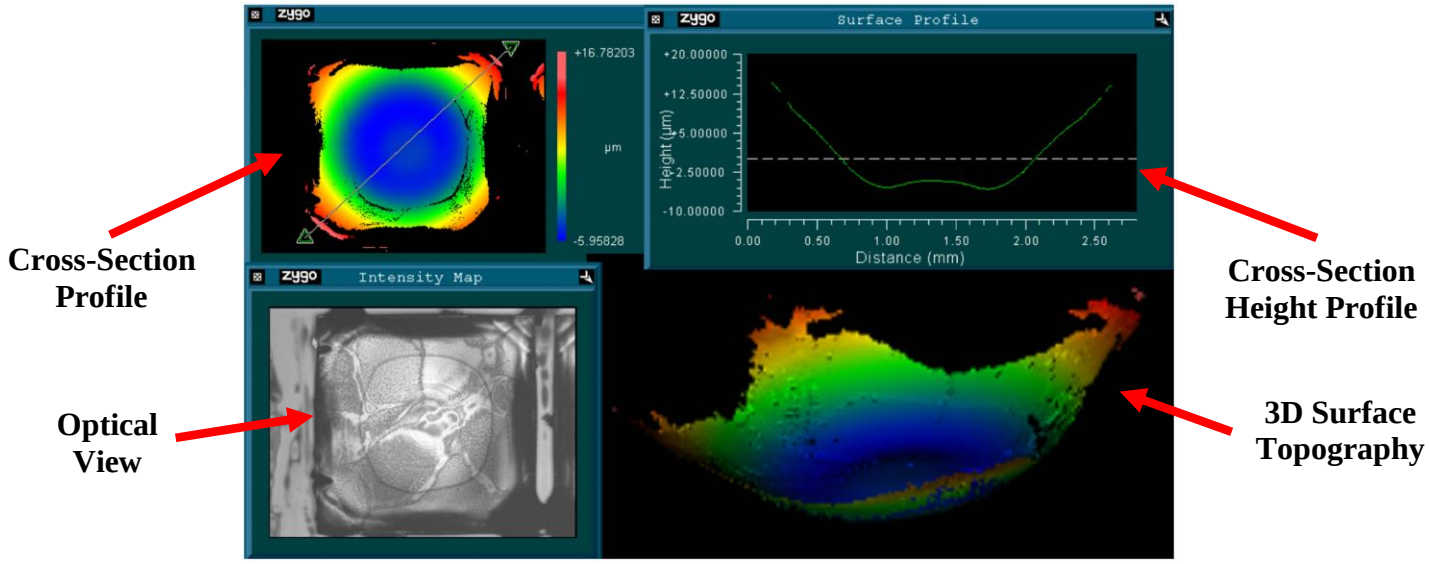

Figure 28: A single 50 mJ/cm^2 MED micromirror with a circular pillar.

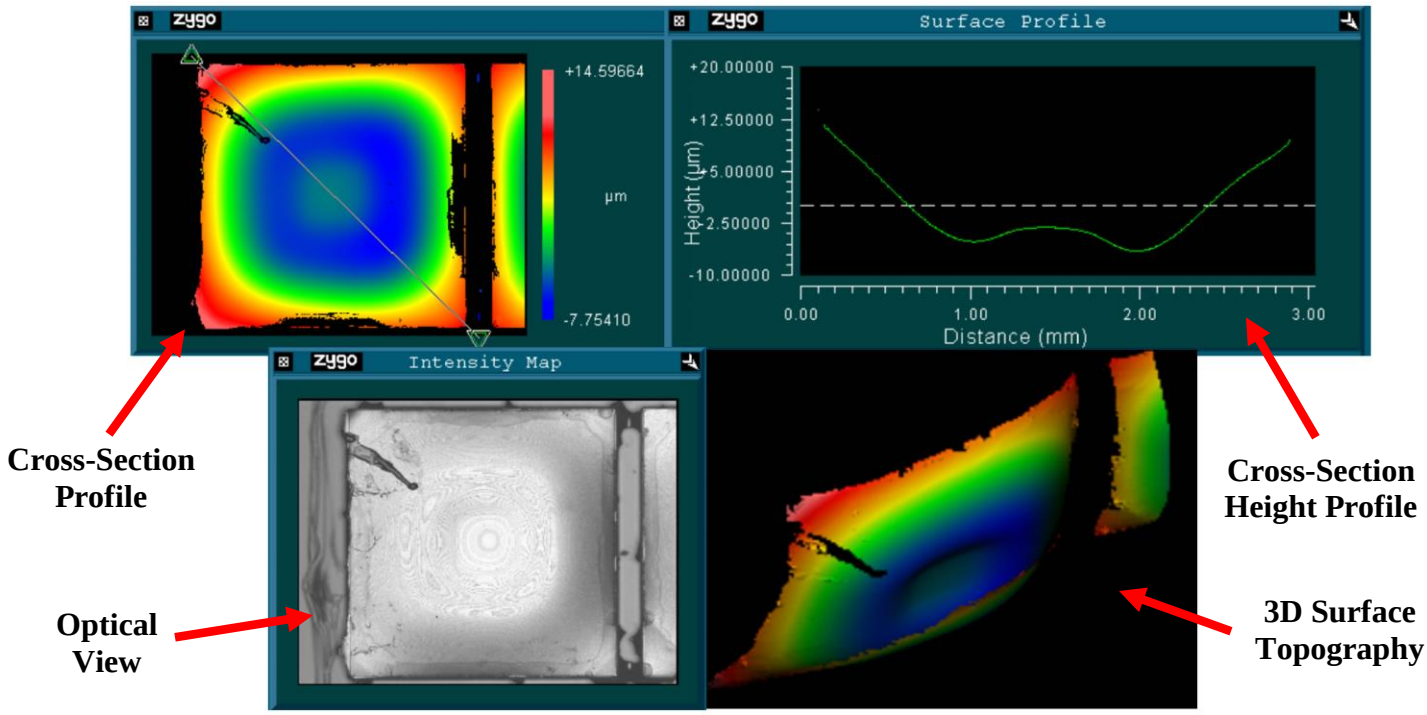

Figure 29: A single 50 mJ/cm^2 MED micromirror with a square pillar.

Figure 30 and 31 shows interferometer images of a single 60 mJ/cm^2 MED with circular and square pillar geometries, respectively. As explained above, the pillar geometry is affecting how the pillar releases. Again, it is seen here that a square pillar is preferred over a circular one.

The cross-section profile for the micromirror with a square pillar, Figure 31, is complete and can be seen in the 3D surface topography. Finally, as the MED increases, from 30 to 60 mJ/cm^2, the overall cross-section profile and 3D surface topography improves making a continuous enough surface that surface profile can be measured, and recoding of that data feasible. Interferometer images showing micromirror arrays for both pillar geometries at 60 mJ/cm^2 MED can be found in Appendix E.

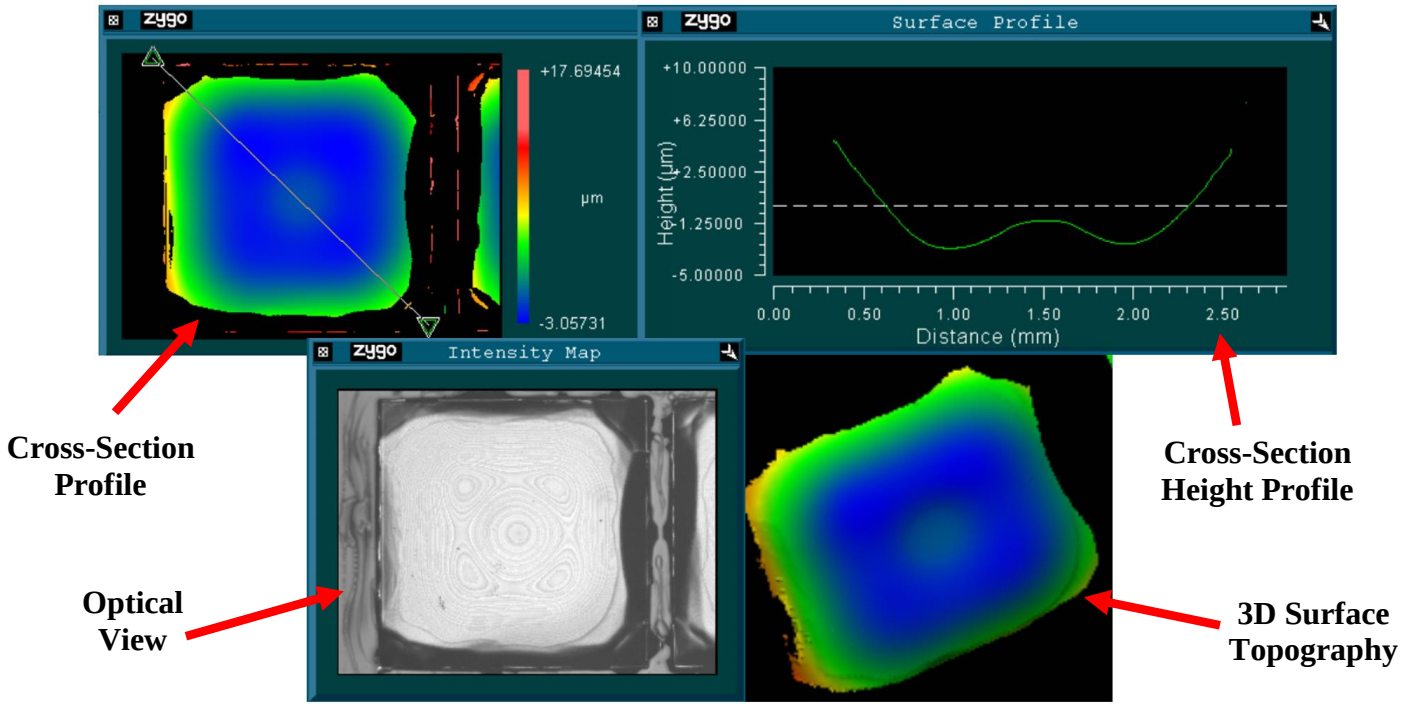

Figure 30: A single 60 mJ/cm^2 MED micromirror with a circular pillar.

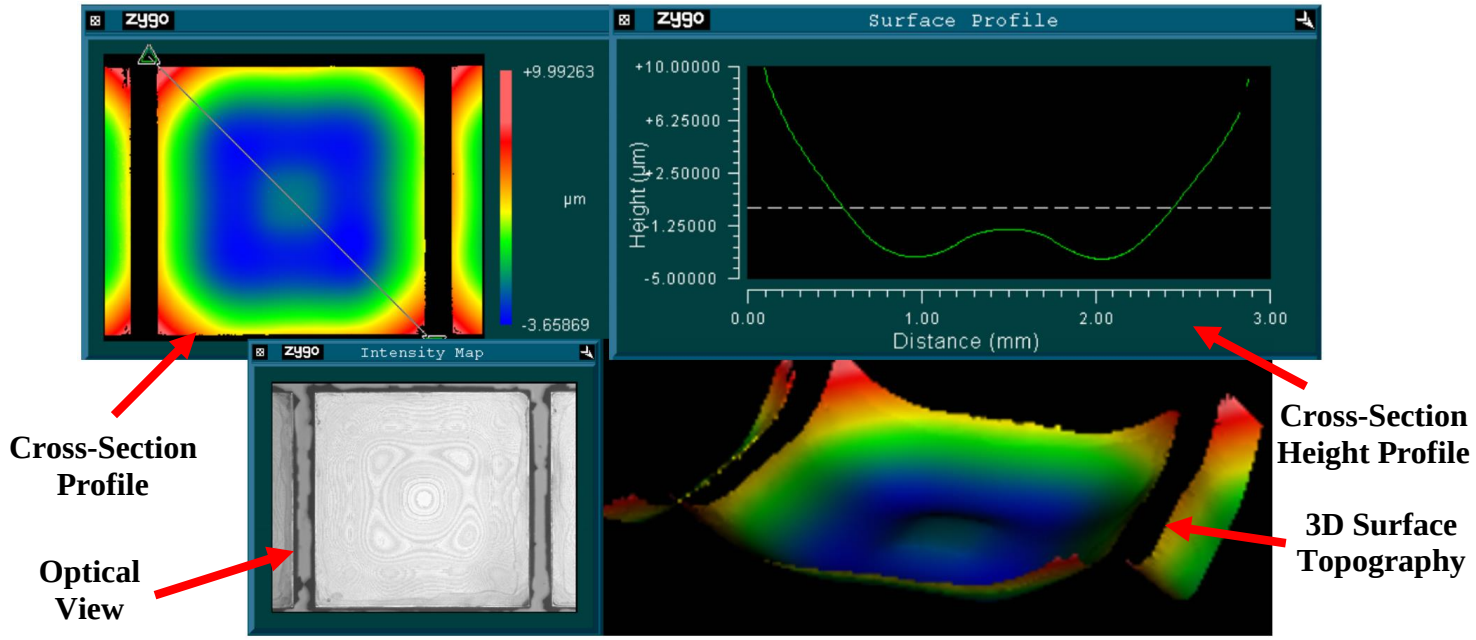

Figure 31: A single 60 mJ/cm^2 MED micromirror with a square pillar.

4.7.3 Statistical Set Up

A 2^2 factorial run was analyzed via Minitab 17. Initially a 2^4 factorial run was set up, but 3 wafers did not yield qualitative results because the interferometer could not effectively collect data on those wafers. The two factors being varied are the MED, 50 & 60 mJ/cm^2, and the pillar geometry, square or circle. All other thicknesses are constant throughout the wafer. Measurement replicates were used without any blocks.

4.7.3.1 Minitab Output

First, the height difference from the pillar to each of the four ends of the mirror is analyzed and can be seen in Figure 32. Four measurements were taken for each micromirror. The Minitab output found that all the factors and their interactions are significant. The output can be seen in Figure 33. The normal plot does not look unusual; therefore, assumptions are not violated. An image of the normal plot can be seen in Figure 34. This output makes sense since the MED directly affects the mirror thickness and depending on that thickness the pillar

geometry will change how the SU-8 developer travels underneath the mirror during the release process.

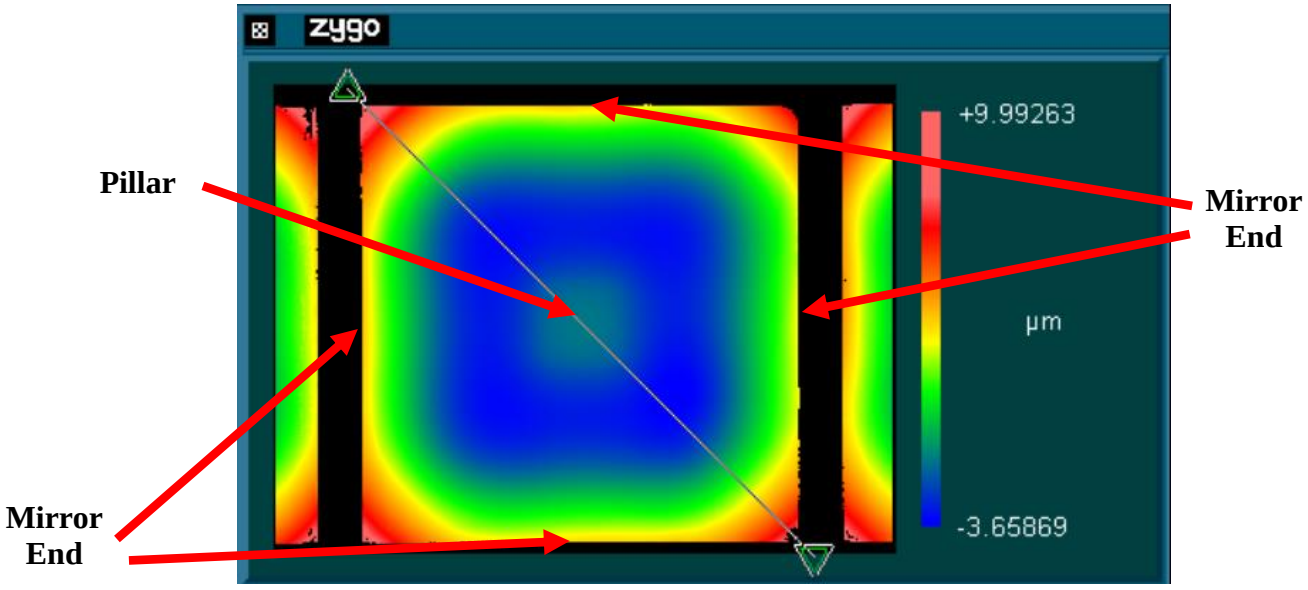

Figure 32: Pillar to side measurement.

Analysis of Variance

Source	DF	Adj SS	Adj MS	F-Value	P-Value
Model	3	1323.4	441.118	120.51	0.000
Linear	2	603.1	301.547	82.38	0.000
MED (mJ/cm^2)	1	355.0	355.028	96.99	0.000
Pillar Geometry	1	229.0	229.042	62.57	0.000
2-Way Interactions	1	172.6	172.563	47.14	0.000
MED (mJ/cm^2)*Pillar Geometry	1	172.6	172.563	47.14	0.000
Error	41	150.1	3.661		
Total	44	1473.4			

Figure 33: Minitab output for the pillar to side measurement.

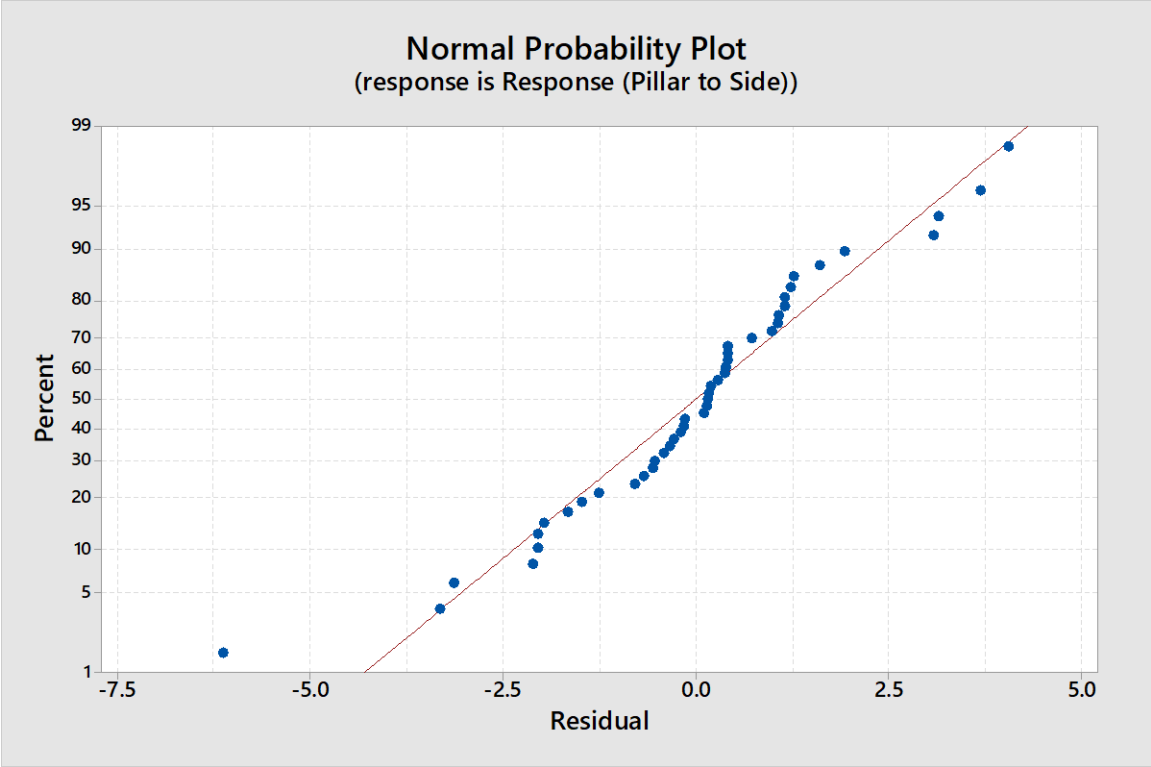

Figure 34: Normal probability plot for pillar to mirror end measurements.

The second measurement to be analyzed is the pillar to mirror corner height difference and can be seen in Figure 35. Four measurements were taken for each micromirror. The Minitab output indicates that only the MED and the two-way interaction between the MED and the pillar geometry are significant factors. The Minitab output can be seen in Figure 36. The normal plot does not look unusual; therefore, assumptions are not violated. An image of the normal plot can be seen in Figure 37. The MED will directly affect the curvature of the mirror; therefore, finding that the geometry of the pillar does not affect that is within reason. The two-way interaction might be significant since the difference in height measurement was taken from the pillar.

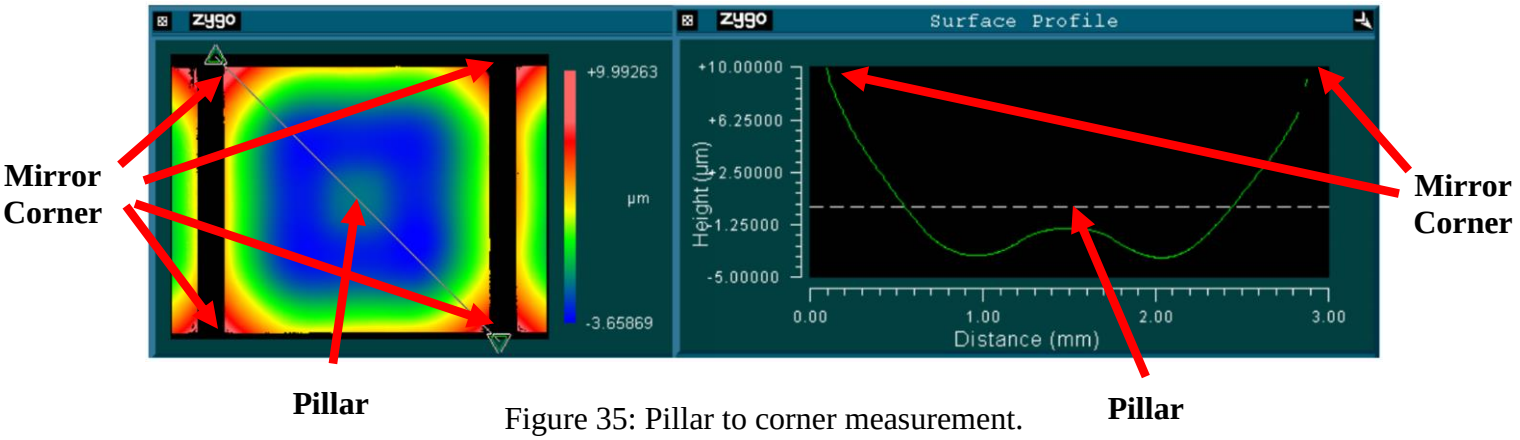

Figure 35: Pillar to corner measurement.

Analysis of Variance

Source	DF	Adj SS	Adj MS	F-Value	P-Value
Model	3	296.962	98.9872	93.14	0.000
Linear	2	42.140	21.0698	19.82	0.000
MED (mJ/cm^2)	1	40.196	40.1956	37.82	0.000
Pillar Geometry	1	0.055	0.0552	0.05	0.824
2-Way Interactions	1	94.770	94.7702	89.17	0.000
MED (mJ/cm^2)*Pillar Geometry	1	94.770	94.7702	89.17	0.000
Error	12	12.754	1.0628		
Total	15	309.716			

Figure 36: Minitab output for the pillar to corner measurement.

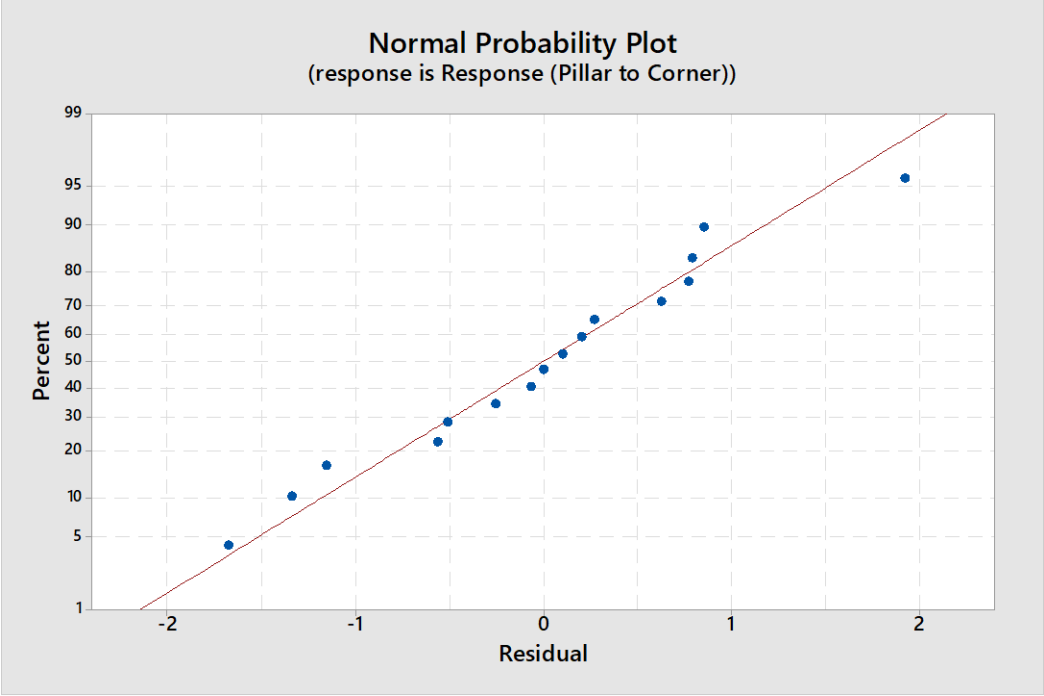

Figure 37: Normal probability plot for pillar to mirror corner measurements.

The final measurement to be analyzed is the pillar to mirror initial dip height difference and can be seen in Figure 38. Four measurements were taken for each micromirror. The Minitab output found that only the pillar geometry and the two-way interaction between the MED and the pillar geometry are significant factors. The Minitab output can be seen in Figure 39. The normal plot does not look unusual; therefore, assumptions are not violated. An image of the normal plot can be seen in Figure 40. The geometry was expected to affect the height difference from the pillar to the initial dip since the pillar is close to the initial dip in the mirror. The two-way interaction is most likely present because the dip is located on the mirror's surface whose thickness is directly affected by the MED. Finally, as stated before the pillar is close to the initial dip in the mirror; therefore, a two-way interaction between the pillar geometry and MED is reasonable in this analysis.

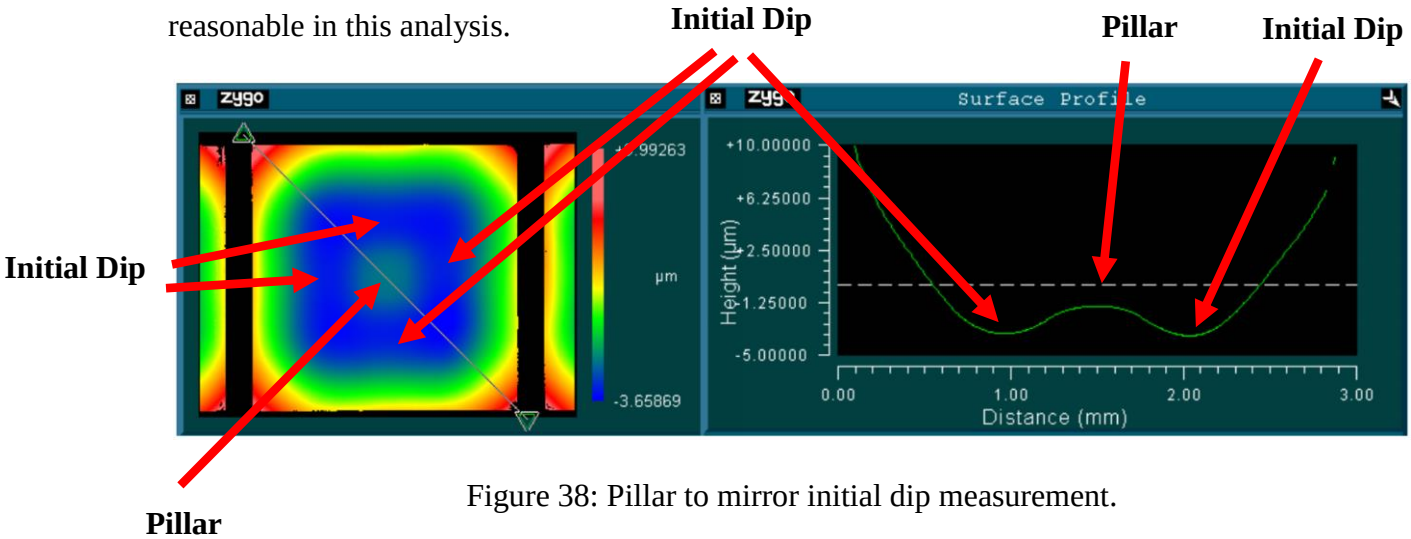

Figure 38: Pillar to mirror initial dip measurement.

Analysis of Variance

Source	DF	Adj SS	Adj MS	F-Value	P-Value
Model	3	3.1001	1.03337	8.72	0.000
Linear	2	1.7843	0.89213	7.53	0.001
MED (mJ/cm^2)	1	0.0673	0.06728	0.57	0.453
Pillar Geometry	1	1.7170	1.71698	14.49	0.000
2-Way Interactions	1	1.3158	1.31585	11.11	0.001
MED (mJ/cm^2)*Pillar Geometry	1	1.3158	1.31585	11.11	0.001
Error	76	9.0031	0.11846		
Total	79	12.1032			

Figure 39: Minitab output for the pillar to first dip measurement.

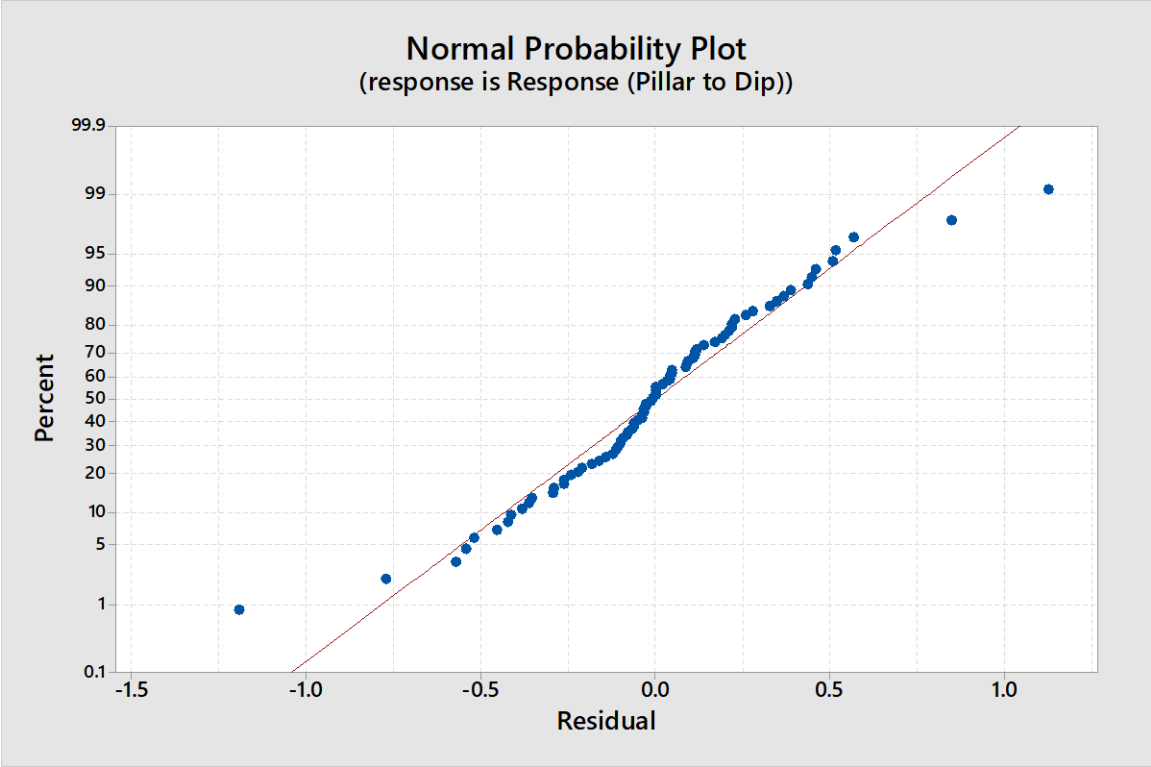

Figure 40: Normal probability plot for pillar to first dip measurements.

Both interferometer and statistical software showed that using a 60 mJ/cm^2 MED with a square pillar structure yields a successful micromirror with a pillar height of 75 μm and mirror thickness of 65 μm. The average step height difference from the pillar to the end of the mirror, pillar to each corner of the mirror, and pillar to initial dip of the mirror is 4.53, 9.22, and 1.51 μm, respectively. Using these averages one can describe an equation of a circle passing through these points as the following: $(x + 15)^2 + (y - 3)^2 = 305$

Table 5 displays the weight of the following four different micromirrors: silicon, SU-8 2050 (60 mJ/cm^2 MED), inverted pyramid (more details in the next section), and inverted pyramid with 30% area reduction. One can see that the micromirrors fabricated in this research are 39.55% lighter than silicon based micromirrors.

Table 5: Weight for Various Micromirrors.

Micromirror	**Weight (g)**	**Weight Difference to Si (%)**
Si	1.35*10-4	N/A
SU-8 2050	8.16*10-5	39.55
Inverted Pyramid	1*10-4	25.93
Inverted Pyramid (30% area reduction)	7*10-5	48.14

Overall, from this final experiment it was found that a double exposure combined with a mirror thickness of about 65 μm and a metal thickness of 1 μm, which were both thick measurements in this research, lead to a micromirror with a conformal metal surface and somewhat flat surface. As a thicker photoresist layer produces a more rigid structure, it's at this thickness that the photoresist has a rigid enough structure to begin to withstand the stress of the metal layer. In addition, a square pillar geometry is favored over a circular pillar geometry. All other micromirrors where thinner layers were used found that the final product yielded a micromirror whose top metal surface was not conformal or flat enough that the interferometer could capture data. Finally, this final fabrication run was reduced from five masks to only three masks (including alignment marks) and two layers; therefore, simplification was achieved.

5.0 Future Recommendations

Several processes in the clean room can range between a minute to several hours. Furthermore, equipment can malfunction and there can be a deficit of materials. These technical difficulties were encountered throughout this research; therefore, this chapter will provide recommendations for future work.

5.1 Interval Exposure

One avenue that was not explored dealt with interval exposure. Instead of only exposing the micromirror twice, experiments could see if there is a significant difference when the mirror is exposed several times creating an inverted pyramid. Having a solid structure from the bottom up could potentially prevent unwanted mirror curvature. A PEB should be done once all exposures are complete.

5.2 Modification to 4.5.1

This method can potentially prove to be successful if a few modifications are made to it. Instead of releasing the structures via a sonic bath they should be released with the hotplate magnetic stirrer. The wafers should be rinsed in a water bath and left out to dry, facing upside down, for a few hours. After the wafers are dry, S1818 should be patterned on the wafers with Mask D. The next step is to do a flood exposure on each wafer, then evaporate gold. The final step is to do a metal liftoff with S1818 solution or SU-8 developer.

5.3 Gold vs Platinum

In the final experiment, platinum was used as the final reflective layer instead of gold. In future experiments it would be worth reattempting gold instead of platinum. This substitution, or in fact possibly other reflective materials, might provide different stresses between the materials. Particularly those which can be deposited without any variations in temperature or other

conditions which would cause expansion or other physical changes to the photoresist layer during deposition. This might lead to better results. In addition, an adhesion layer was never used in conjunction with gold. Having data on both different reflective surfaces might discover new significant findings.

5.4 Sputtering vs Evaporation

In this research, metal sputtering significantly consumed less time than metal evaporation, and it was accessible. Evaporation has a better surface conformality than sputtering and is the preferred method to deposit metals for liftoff; therefore, the final experiment should be redone and utilize metal evaporation opposed to sputtering.

5.5 Atomic Layer Deposition

The final experiment should end with an atomic layer deposition. This deposition would uniformly coat the whole structure with gold. This would guarantee the flow of heat from the top of the mirror surface to the base of the micromirror.

5.6 Other Potential Applications

The multiple exposure technique used in this thesis could be used to make sophisticated structures. While initially a single patterned pillar led to the attempt to build a more complex structure through two exposures, this process could be extended. Multiple intermediate steps could be used to make an inverted pyramidal structure which might provide enough support to hold the metal layer more successfully as a mirror surface. Additionally, this approach with additional layers of SU-8 could in turn build even more complex structures similar to those made in additive manufacturing processes.

Appendix A. Initial Design Fabrication Process Follower

The steps outlined in the fabrication process follower can be seen in Figure 9. The initial design fabrication process follower can be seen in Figure 41. Note that the thicknesses outlined in the process follower are the thinnest they will be. The middle layer will reach a thickness of 2 μm, and the bottom and upper gold layers will each reach a thickness of 300 nm.

	INSPECT WAFER: ☐ Note any defects	**Start Date** **Start Time**	
	SOLVENT CLEAN WAFER (INITIAL CLEANING IF NECESSARY): ☐ 30 sec acetone rinse at 500 rpm ☐ 30 sec methanol rinse at 500 rpm ☐ 30 sec DI water rinse at 500 rpm ☐ Dry with nitrogen at 500 rpm		
	DEHYDRATION BAKE: ☐ 1 min 110°C hot plate bake		
	Make Alignment Marks		
	S1818 COAT, 2 μm: ☐ Flood wafer with 1818 ☐ 30 sec spin at 4,000 rpm, ramp=200 rpm/s ☐ 75 sec 110°C hot plate bake		
	EXPOSE S1818 WITH MASK A: ☐ 7.0 sec exposure using EVG 620; 4 sec exposure using MJB3		
	S1818 DEVELOP: ☐ 40 sec develop with 351:DI (1:5), use a spin method at 500 rpm ☐ 30 sec DI water rinse at 500 rpm ☐ Dry with nitrogen at 500 rpm		
	ALIGNMENT MARK DEPOSITION: ☐ *Evaporate* 40 nm Ti and then 200 nm Au		
	LIFT-OFF METAL: ☐ Tape lift off *evaporated* Ti/Au ☐ Acetone sonic bath until all S1818 is removed ☐ Solvent clean wafer		
	Begin Making the 25 μm Pillar of the Mirror		
	SU-8-2025 COAT, 25 μm: ☐ Flood wafer with SU-8-2025 ☐ 30 sec spin at 3,000 rpm, ramp=500 rpm/s for 5 sec @ 100 rpm/sec accel ☐ 3 min 95°C hot plate soft bake		
	EXPOSE SU-8-2025 WITH MASK B: ☐ Exposure using EVG 620		
	Bottom 100 nm Gold Layer of Mirror		
	S1818 COAT, 2 μm: ☐ Flood wafer with 1818 ☐ 30 sec spin at 4,000 rpm, ramp=200 rpm/s ☐ 75 sec 110°C hot plate bake		
	EXPOSE S1818 WITH MASK C: ☐ 7.0 sec exposure using EVG 620; 4 sec exposure using MJB3		
	S1818 DEVELOP: ☐ 40 sec develop with 351:DI (1:5), use a spin method at 500 rpm ☐ 30 sec DI water rinse at 500 rpm ☐ Dry with nitrogen at 500 rpm		
	BOTTOM MIRROR LAYER METAL DEPOSITION: ☐ *Evaporate* 75 nm Au		

	LIFT-OFF METAL: ☐ Tape lift off *evaporated* Au along alignment marks ☐ Acetone sonic bath until S1818 is removed ☐ Solvent clean wafer		
	Middle 250 nm SU-8-2002 Mirror Layer	SiO_2 will later be used instead of SU-8-2002 in some samples	
	SU-8-2002 COAT, 250 nm: ☐ Dilute SU-8-2002 resist with 2.5 equivalents of SU-8-2000 thinner/methanol ☐ Flood wafer with SU-8-2002 ☐ 60 sec spin at 2,000 rpm, ramp=200 rpm/s ☐ 75 sec 110°C hot plate soft bake		
	EXPOSE SU-8-2002 WITH MASK D: ☐ Exposure using EVG 620		
	SU-8-2002 POST BAKE: ☐ 75 sec 110°C hot plate post exposure bake		
	SU-8-2002 DEVELOP: ☐ SU-8 developer for **less than a minute** (other solvent based developers such as ethyl lactate and diacetone alcohol may be used) ☐ Spray/wash with Isopropyl Alcohol for another 10 sec ☐ Air dry with nitrogen		
	Final 100 nm Top Gold Layer		
	S1818 COAT, 2 μm: ☐ Flood wafer with 1818 ☐ 30 sec spin at 4,000 rpm, ramp=200 rpm/s ☐ 75 sec 110°C hot plate bake		
	EXPOSE S1818 WITH MASK C: ☐ 7.0 sec exposure using EVG 620; 4 sec exposure using MJB3		
	S1818 DEVELOP: ☐ 40 sec develop with 351:DI (1:5), use a spin/stop/spin/stop method at 500 rpm ☐ 30 sec DI water rinse at 500 rpm ☐ Dry with nitrogen at 500 rpm		
	TOP MIRROR LAYER METAL DEPOSITION: ☐ *Evaporate* 75 nm Au		
	LIFT-OFF METAL: ☐ Tape lift off *evaporated* Au along alignment marks ☐ Acetone sonic bath until S1818 is removed ☐ Solvent clean wafer		
	S1818 COAT, 2 μm (1mm x 1mm WET ETCH): ☐ Flood wafer with 1818 ☐ 30 sec spin at 4,000 rpm, ramp=200 rpm/s ☐ 75 sec 110°C hot plate bake		
	EXPOSE S1818 WITH MASK E (1mm x 1mm): ☐ 7.0 sec exposure using EVG 620; 4 sec exposure using MJB3		
	S1818 DEVELOP: ☐ 40 sec develop with 351:DI (1:5), use a spin/stop/spin/stop method at 500 rpm ☐ 30 sec DI water rinse at 500 rpm ☐ Dry with nitrogen at 500 rpm		
	FLOOD EXPOSURE: ☐ 300 sec DUV exposure	Need to make sure S1818 is releasable in the end after metal wet etch	

	METAL WET ETCH: ☐ Need to etch through 200 nm of Au using Au etchant ☐ Refer to the etch rate of etchant to find appropriate time		
	S1818 DEVELOP: ☐ 40 sec develop with 351:DI (1:5), use a spin/stop/spin/stop method at 500 rpm ☐ 30 sec DI water rinse at 500 rpm ☐ Dry with nitrogen at 500 rpm		
	SU-8-2025 DEVELOP: ☐ SU-8 developer for 4 min (other solvent based developers such as ethyl lactate and diacetone alcohol may be used) ☐ Spray/wash with Isopropyl Alcohol for another 10 sec ☐ Air dry with nitrogen		

Figure 41: Initial design fabrication process follower.

Appendix B. Initial Design Masks

The fabrication masks are designed via the MEMS software L-EDIT. An illustration of the masks can be found in Figure 9. Light travels through where figures are drawn in Masks A, B, and D, and can be seen in Figures 42, 43, and 44, respectively. It is important to note that Mask B has circular and rectangular shapes, which creates two geometrically different pillars. Masks C and E are fabricated with the opposite polarity of Mask A, B, and D, and can be seen in Figures 45 and 46, respectively. This means that light does not travel through where figures are drawn.

Figure 42: The first mask, Mask A.

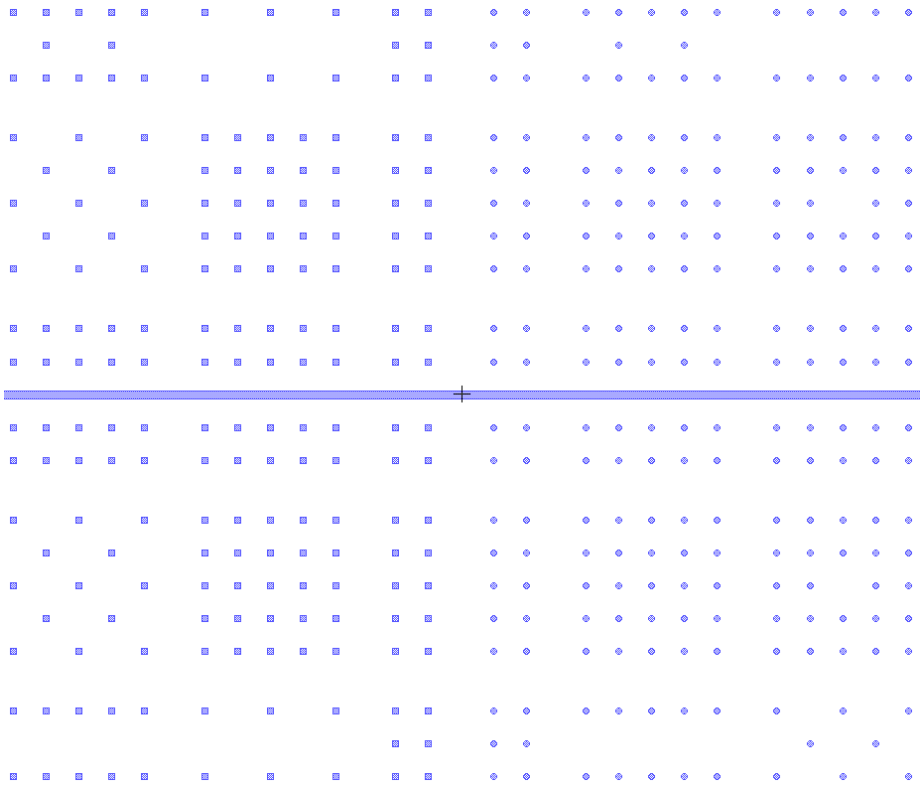

Figure 43: The second mask, Mask B.

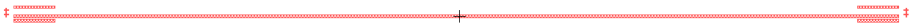

Figure 44: The third mask, Mask C.

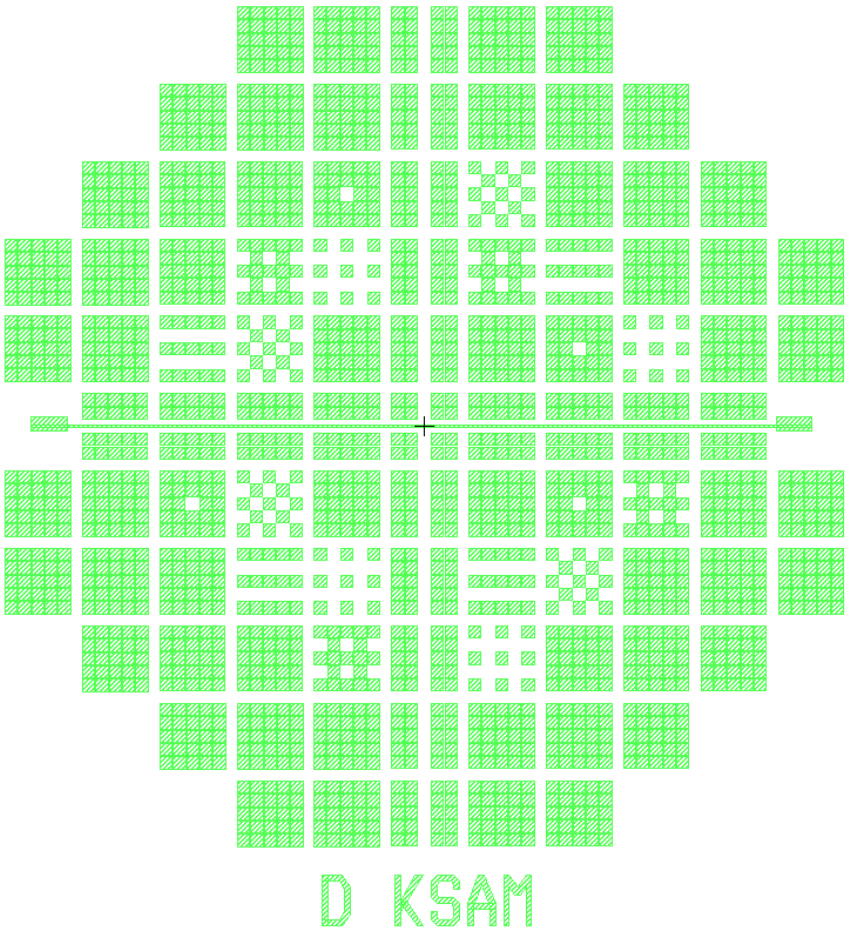

Figure 45: The fourth mask, Mask D.

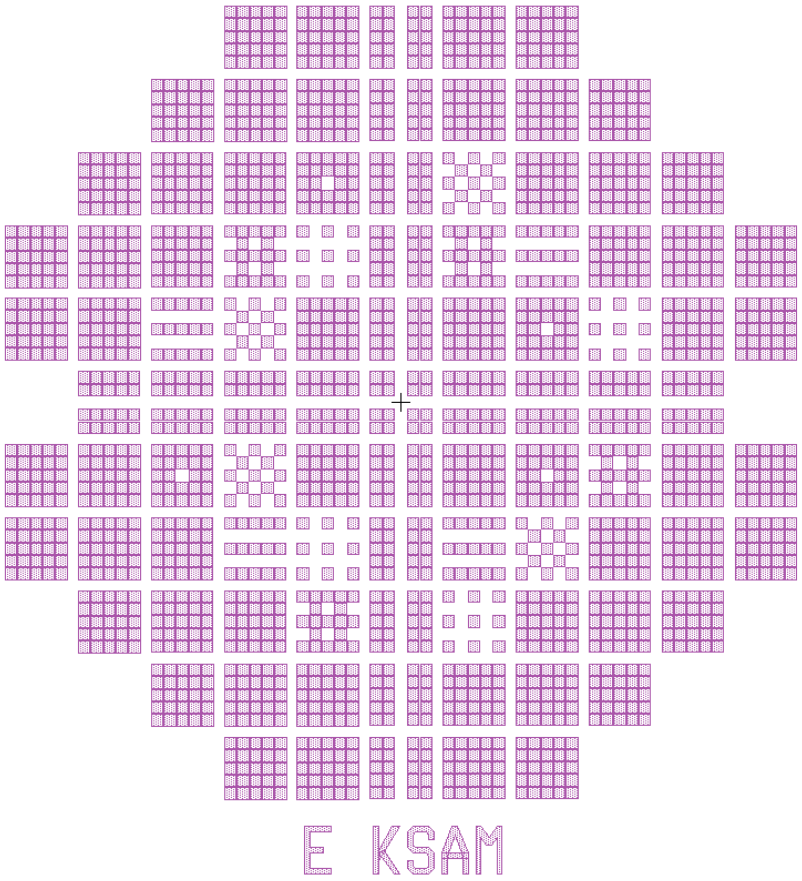

Figure 46: The fifth mask, Mask E.

Appendix C. Initial Design Experimental Set Up via Minitab 17

Figure 47 shows the randomized runs that were obtained via Minitab 17. A, B, C, and D represent the four factors that are explained in section 3.2.2. Those four factors are arbitrarily assigned. 8 wafers are used to represent each run since Mask B, seen in Appendix B, creates both circular and rectangular pillars. Each wafer has arrays of micromirrors that all have the same thicknesses for each respective layer; therefore, replicate responses of each run are used in the analysis.

Full Factorial Design

Factors:	4	Base Design:	4, 16
Runs:	16	Replicates:	1
Blocks:	1	Center pts (total):	0

All terms are free from aliasing.

Design Table (randomized)

Run	A	B	C	D
1	+	+	−	+
2	−	+	−	−
3	−	−	+	+
4	+	−	−	+
5	−	+	+	−
6	+	−	+	+
7	−	+	−	+
8	−	−	−	−
9	−	−	−	+
10	−	+	+	+
11	+	+	+	+
12	+	−	−	−
13	+	+	+	−
14	−	−	+	−
15	+	−	+	−
16	+	+	−	−

Figure 47: Randomized design table for 2^4 factorial design.

Appendix D. Final Design Fabrication Process Follower

The final step by step detailed design fabrication process follower can be seen in Figure 48. An explanation of the fabrication process follower can be found in section 4.7.

INSPECT WAFER:
- ☐ Note any defects

SOLVENT CLEAN WAFER (INITIAL CLEANING IF NECESSARY):
- ☐ 30 sec acetone rinse at 500 rpm
- ☐ 30 sec methanol rinse at 500 rpm
- ☐ 30 sec DI water rinse at 500 rpm
- ☐ Dry with nitrogen at 500 rpm

DEHYDRATION BAKE:
- ☐ 1 min 110°C hot plate bake

Make Alignment Marks

S1818 COAT, 2 μm:
- ☐ Flood wafer with 1818
- ☐ 30 sec spin at 4,000 rpm, ramp=200 rpm/s
- ☐ 75 sec 110°C hot plate bake

EXPOSE S1818 WITH MASK A:
- ☐ 7.0 sec exposure using EVG 620; 4 sec exposure using MJB3

S1818 DEVELOP:
- ☐ 40 sec develop with 351:DI (1:5), use a spin method at 500 rpm
- ☐ 30 sec DI water rinse at 500 rpm
- ☐ Dry with nitrogen at 500 rpm

ALIGNMENT MARK DEPOSITION:
- ☐ *Evaporate* 40 nm Ti and then 200 nm Au

LIFT-OFF METAL:
- ☐ Tape lift off *evaporated* Ti/Au
- ☐ Acetone sonic bath until all S1818 is removed
- ☐ Solvent clean wafer

Single 140 μm Micromirror Layer

SU-8-2050 COAT, 140 μm:
- ☐ Flood wafer with SU-8 2050
- ☐ 30 sec spin at 1,000 rpm, ramp=500 rpm/s for 5 sec @ 100 rpm/sec accel
- ☐ 7 min 65°C hot plate soft bake
- ☐ 45 min 95^oC hot plate soft bake

EXPOSE SU-8-2050 WITH MASK D:
- ☐ Expose with 60 mJ/cm^2

EXPOSE SU-8-2050 WITH MASK B:
- ☐ Expose with 370 mJ/cm^2

SU-8-2050 PEB:
- ☐ 5 min 65°C hot plate bake
- ☐ 15 min 95^oC hot plate bake

Top 1 μm Metal Deposition

TOP MIRROR LAYER METAL DEPOSITION:
- ☐ *Sputter* a few nm Cr + 1 μm Al + a few nm Cr + a few nm Pt

Single Layer Liftoff

SLL VIA SONIC BATH:

- ☐ Place wafer in petri dish filled with SU-8 developer
- ☐ Place petri dish in sonic bath filled with water
- ☐ Leave in sonic bath for approximately 30 minutes

Hot Plate Magnetic Stirrer Release

Release:

- ☐ Place magnetic stirrer inside 500 mL beaker filled with 150 mL of SU-8 developer
- ☐ Place wafer, facing up, inside beaker
- ☐ Set hot place stirrer to 180 rpm and allow the devices to release for 160 minutes
- ☐ Rinse wafer in petri dish filled with water
- ☐ Allow wafer to dry over a few hours by placing it upside down, balanced between two wafer holders on each end, in the clean room

Figure 48: Final design fabrication process follower.

Appendix E. Micromirror Array Interferometer Images

Interferometer images of micromirror arrays with circular and square pillar geometries at 30, 40, 50, and 60 mJ/cm^2 MEDs can be seen below. These zoomed out images are supplementary to those seen in section 4.7.2.

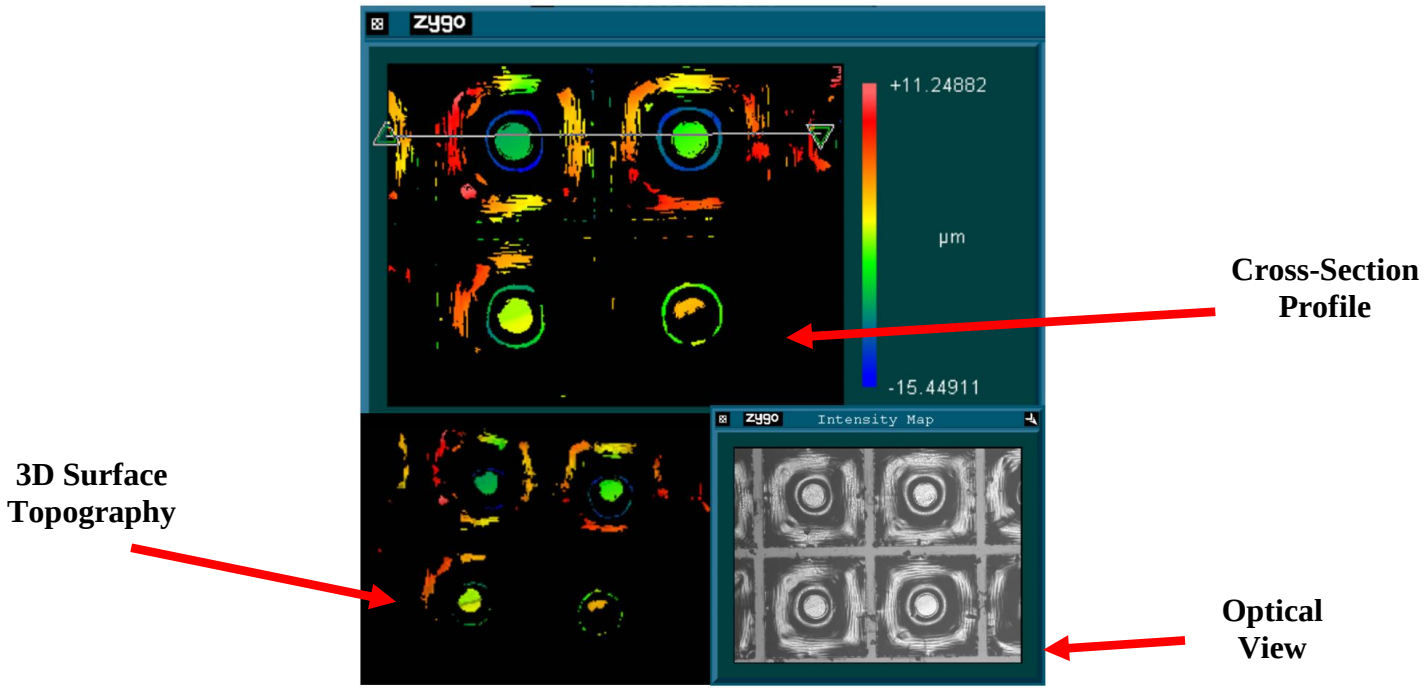

Figure 49: An array of 30 mJ/cm^2 MED micromirrors with circular pillars.

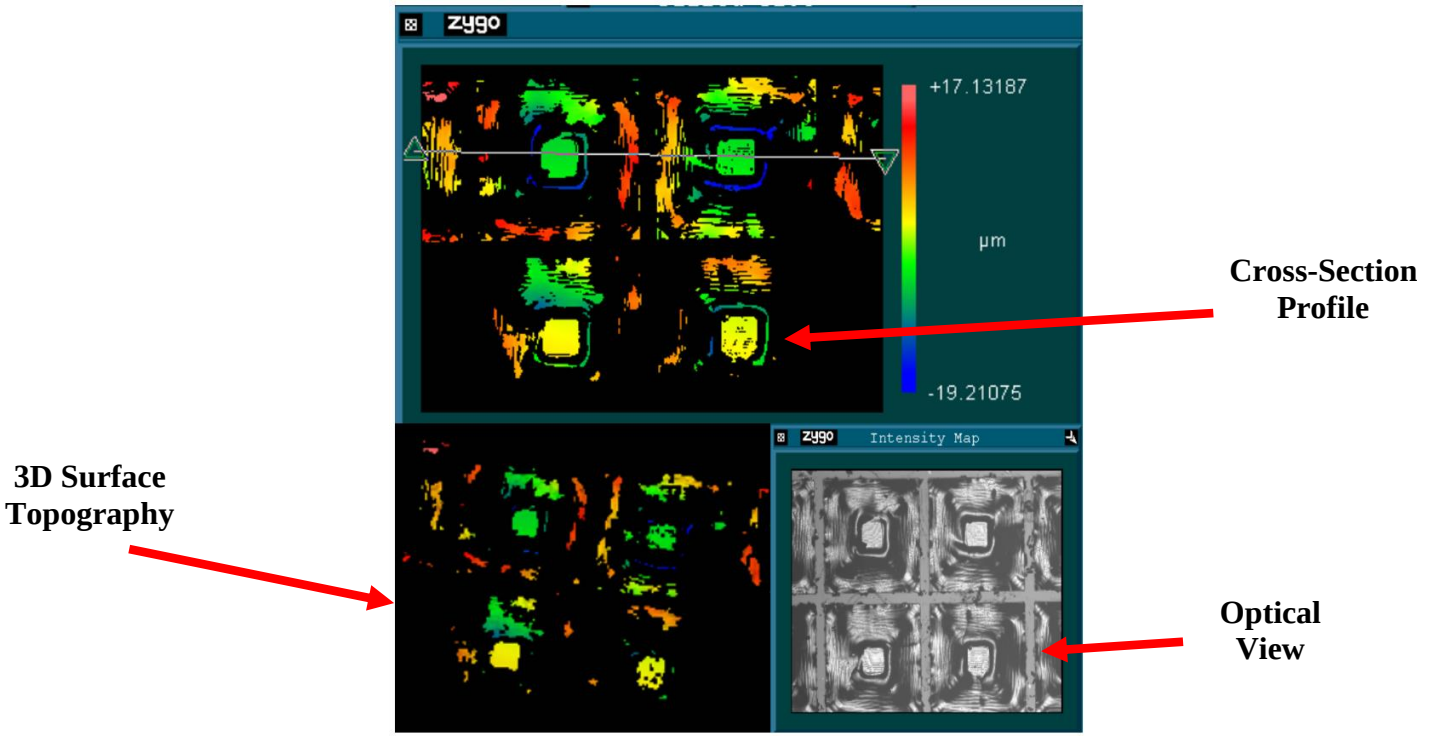

Figure 50: An array of 30 mJ/cm^2 MED micromirrors with square pillars.

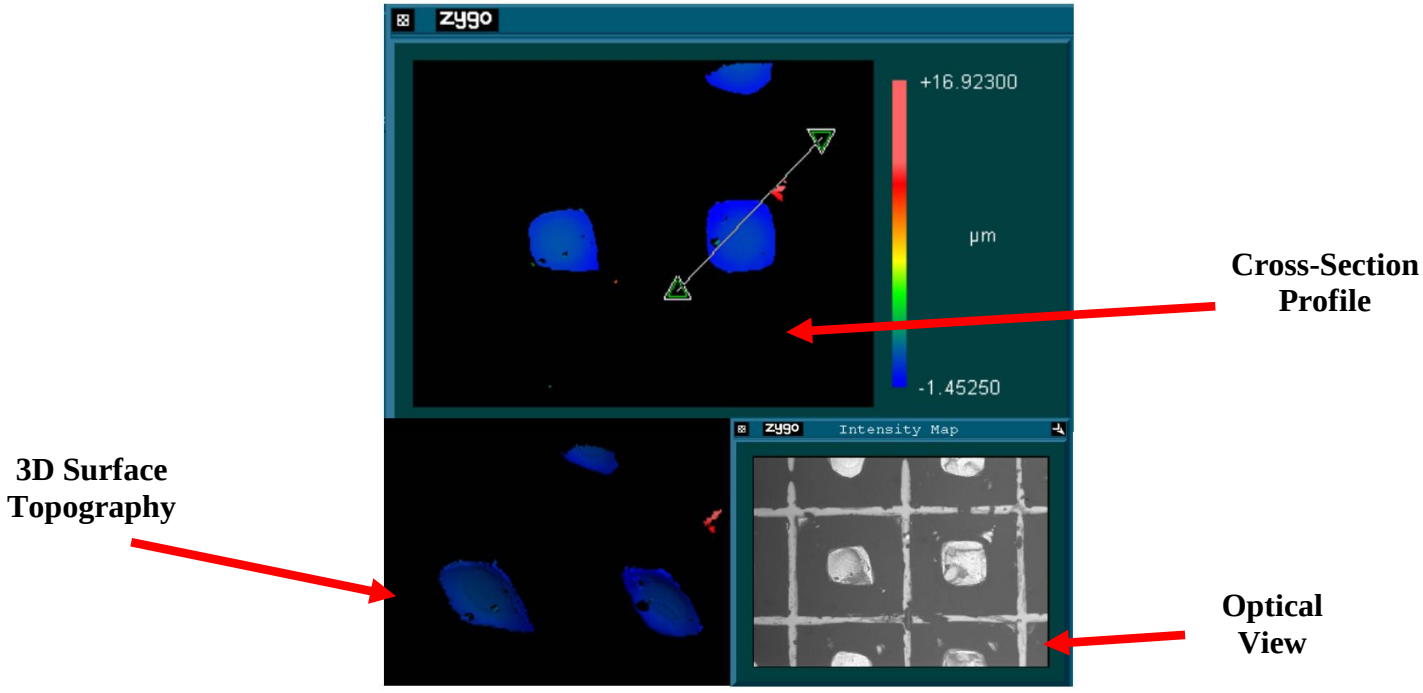

Figure 51: An array of 40 mJ/cm^2 MED micromirrors with circular pillars.

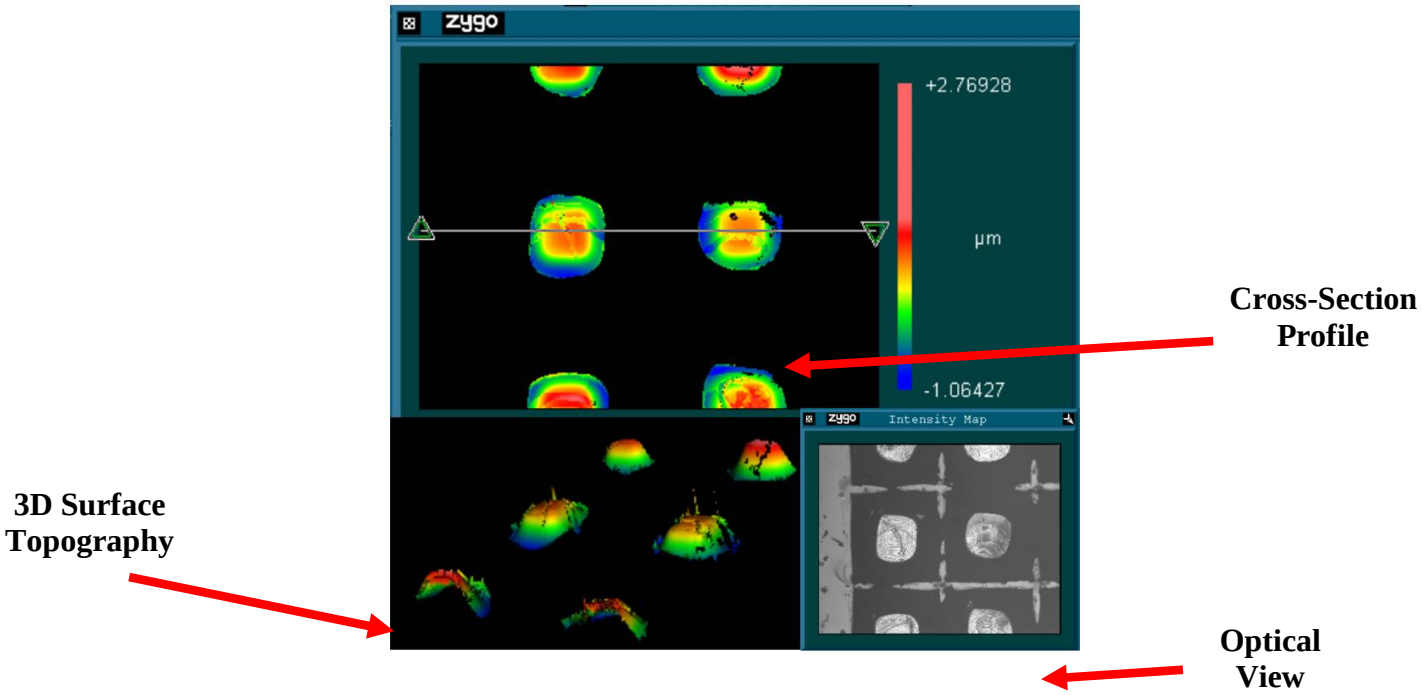

Figure 52: An array of 40 mJ/cm^2 MED micromirrors with square pillars.

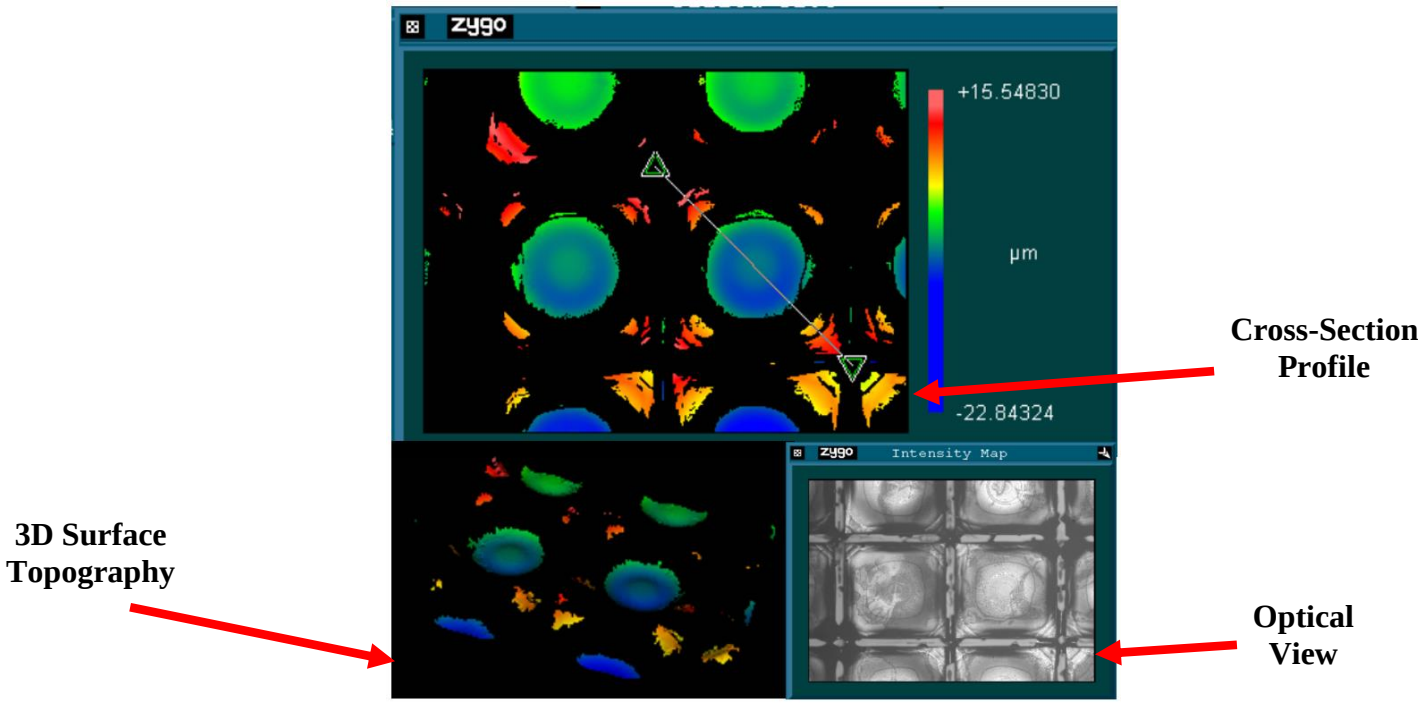

Figure 53: An array of 50 mJ/cm^2 MED micromirrors with circular pillars.

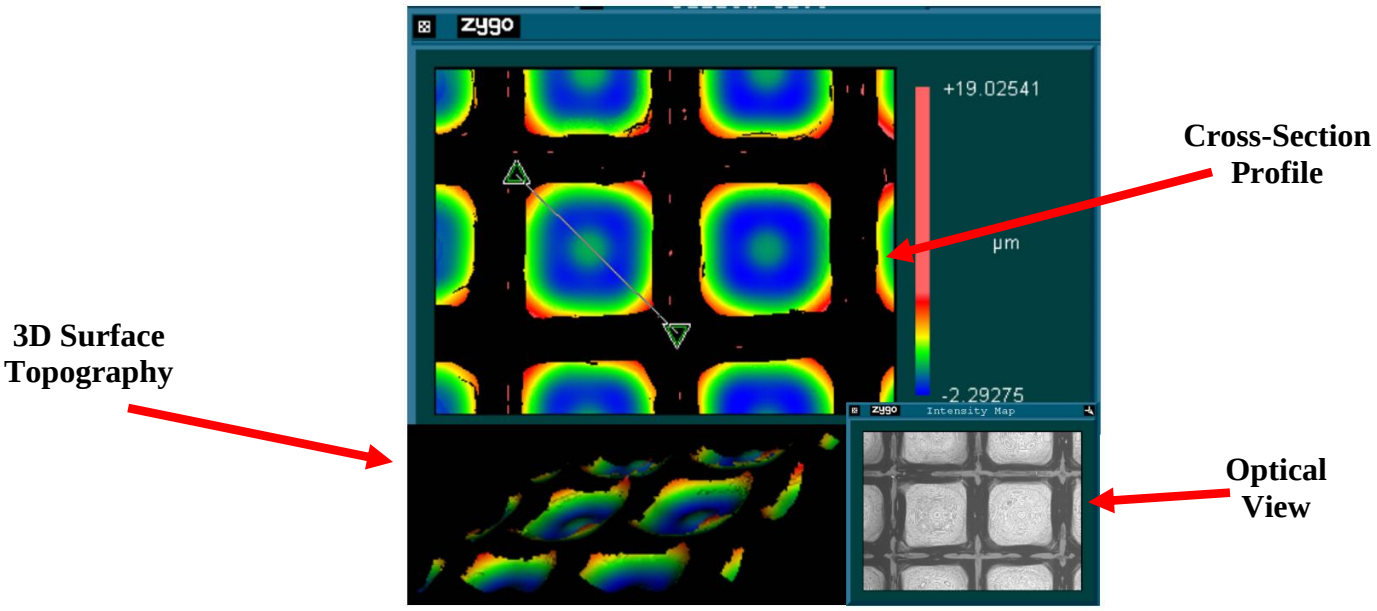

Figure 54: An array of 50 mJ/cm^2 MED micromirrors with square pillars.

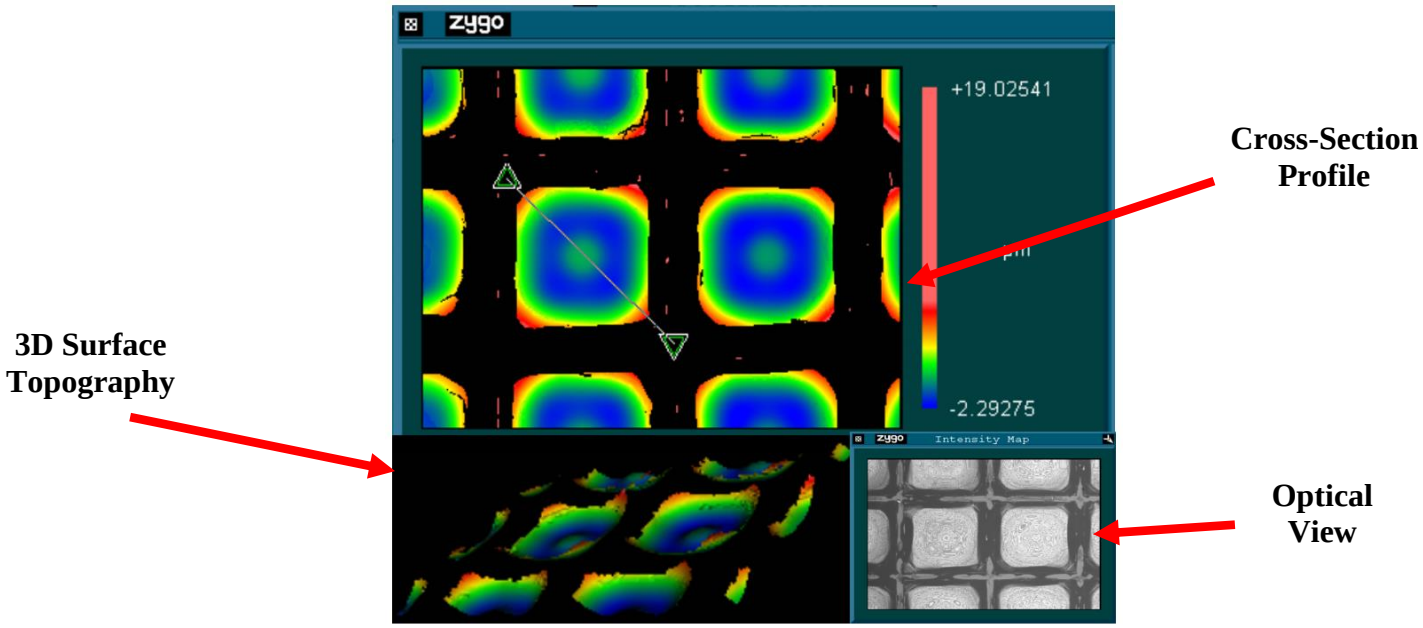

Figure 55: An array of 60 mJ/cm^2 MED micromirrors with circular pillars.

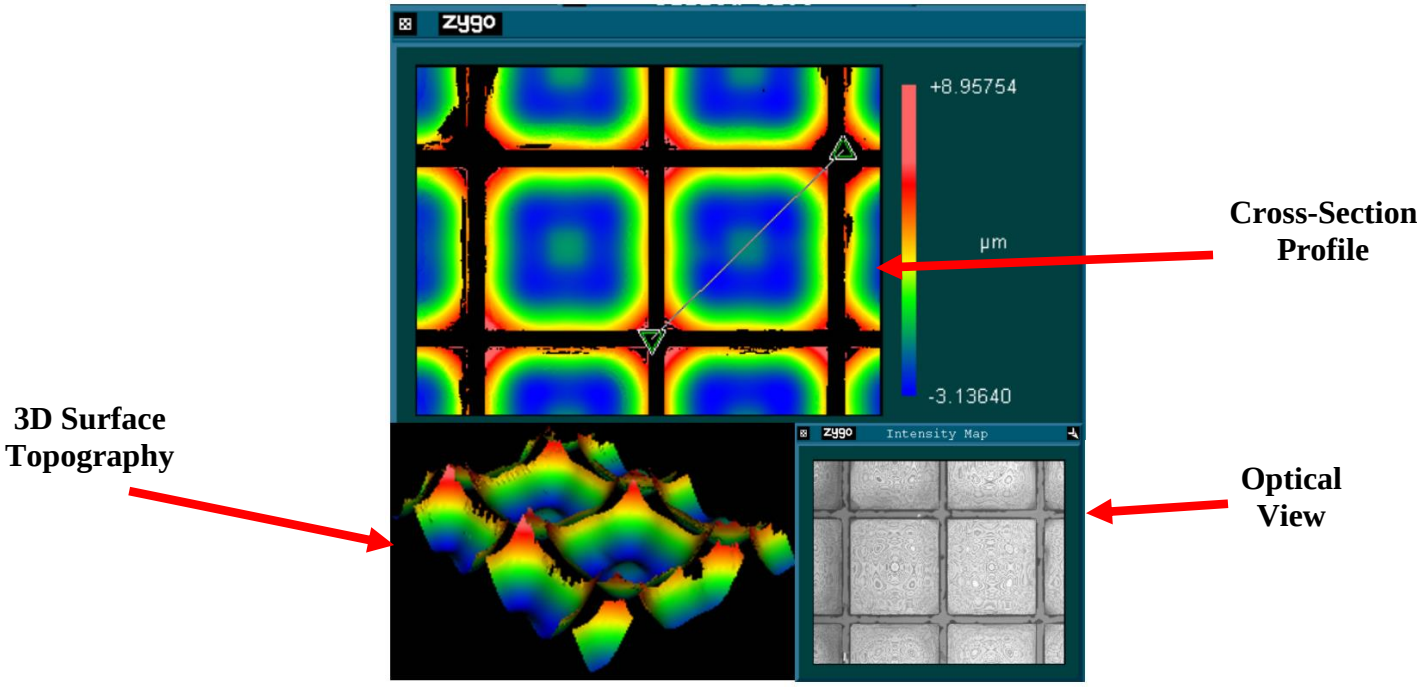

Figure 56: An array of 60 mJ/cm^2 MED micromirrors with square pillars.

BIBLIOGRAPHY

[1] N. E. Glavitz, L. A. Starman, R. A. Coutu, and R. L. Johnston, "Effects of SU-8 cross-linking on flip-chip bond strength when assembling and packaging MEMS," *Procedia Eng.*, vol. 25, pp. 471–474, 2011.

[2] L. Starman, J. Walton, H. Hall, and R. Lake, "Post Fabrication Processing of Foundry MEMS Structures Exhibiting Large, Out-of-Plane Deflections," *Proceedings*, vol. 1, no. 5, p. 553, 2017.

[3] K. W. Waggoner, "SEGMENTED CONTROL OF ELECTROSTATICALLY."

[4] J. Khoury and J. Vella, "Optically addressed deformable mirror for low-light applications," *J. Micro/Nanolithography, MEMS, MOEMS*, vol. 14, no. 4, p. 41312, 2015.

[5] SCME, "Introduction to Transducers, Sensors, and Actuators," *Southwest Cent. Microsystems Educ. Univ. New Mex.*, p. 4, 2014.

[6] K. B. Lee, *Principles of Microelectromechanical Systems*. 2010.

[7] S. A. Campbell, "Fabrication Engineering at the Micro-and Nanoscale (The Oxford Series in Electrical and Computer Engineering)," 2012.

[8] NATO, *MEMS Aerospace Applications*, vol. 323, no. October 2002. 2004.

[9] R. S. Mullins and T. I. Kamins, "Device electronics for integrated circuits." New York, NY: John Wiley & Sons Inc, 2003.

[10] D. Koester, A. Cowen, R. Mahadevan, M. Stonefield, and B. Hardy, "PolyMUMPs design handbook," *MEMSCAP Inc*, 2003.

[11] R. C. Jaeger, *Introduction to Microelectronic Fabrication: Volume 5 of Modular Series on Solid State Devices*, vol. 2. Prentice Hall Upper Saddle River, 2001.

[12] K. Microchem, "SU-8 3000 Permanent Epoxy Negative Photoresist," *Data Sheet*, 2006.

[13] MEMSCAP, “PolyMUMPs and MEMS Multi Project Wafer Service.” [Online]. Available: http://www.memscap.com/products/mumps/polymumps. [Accessed: 21-Dec-2018].

[14] J. P. Walton, R. A. Coutu Jr., and L. Starman, “Modeling and simulations of new electrostatically driven, bimorph actuator for high beam steering micromirror deflection angles,” *MOEMS Miniaturized Syst. XIV*, vol. 9375, p. 93750Y, 2015.

[15] K. Waggoner, “Segmented Control of Electrostatically Actuated Bimorph Micromirrors,” Air Force Institute of Technology, 2017.

[16] D. C. Montgomery, *Design and analysis of experiments*. John wiley & sons, 2017.

REPORT DOCUMENTATION PAGE

Form Approved
OMB No. 074-0188

1. REPORT DATE *(DD-MM-YYYY)*	2. REPORT TYPE	3. DATES COVERED *(From – To)*
21-03-2019	Master's Thesis	August 2018 – March 2019

TITLE AND SUBTITLE

Improved Fabrication for Micromirror Arrays

5a. CONTRACT NUMBER

5b. GRANT NUMBER

5c. PROGRAM ELEMENT NUMBER

6. AUTHOR(S)

Enoc Flores, Second Lieutenant, USAF

5d. PROJECT NUMBER

5e. TASK NUMBER

5f. WORK UNIT NUMBER

7. PERFORMING ORGANIZATION NAMES(S) AND ADDRESS(S)
Air Force Institute of Technology
Graduate School of Engineering and Management (AFIT/EN)
2950 Hobson Way, Building 640
WPAFB OH 45433-8865

8. PERFORMING ORGANIZATION REPORT NUMBER

AFIT-ENG-MS-19-M-027

9. SPONSORING/MONITORING AGENCY NAME(S) AND ADDRESS(ES)
Intentionally left blank

10. SPONSOR/MONITOR'S ACRONYM(S)

11. SPONSOR/MONITOR'S REPORT NUMBER(S)

12. DISTRIBUTION/AVAILABILITY STATEMENT
DISTRUBTION STATEMENT A. APPROVED FOR PUBLIC RELEASE; DISTRIBUTION UNLIMITED.

13. SUPPLEMENTARY NOTES
This material is declared a work of the U.S. Government and is not subject to copyright protection in the United States.

14. ABSTRACT

Micromirror devices which consisted of one SU-8 2050 layer, two different exposures, and a series of metal depositions were constructed and evaluated. By varying the exposure, a micromirror structure was fabricated with different thicknesses, a ratio of 1.083 $\mu m/(\frac{mJ}{cm^2})$ was found. The initial design consisted of four layers. The pillar was made of one SU-8 layer, and the top portion had three layers in the following order: gold, SU-8, and gold. This design could not be released and did not have characteristics of a flat and conformal reflective surface. Several variations of the initial design were explored and all of them lacked a flat and conformal top reflective surface. Both interferometric and statistical software showed that using a 60 mJ/cm^2 mirror exposure dosage and a 370 mJ/cm^2 square pillar exposure dosage yields a micromirror with a conformal top reflective surface. The length and width of the pillars are 200μm by 200μm, with a height of 75 μm. The mirror's length and width are 1 mm by 1 mm, and the thickness is 65 μm. The average step height difference from the pillar to the side of the mirror, pillar to each corner of the mirror, and pillar to initial dip in the mirror is 4.53, 9.22, and 1.51 μm, respectively.

15. SUBJECT TERMS
mems micromirrors, su-8

16. SECURITY CLASSIFICATION OF:			17. LIMITATION OF ABSTRACT	18. NUMBER OF PAGES	19a. NAME OF RESPONSIBLE PERSON
a. REPORT	b. ABSTRACT	c. THIS PAGE			Tod Laurvick, Major, PhD, USAF AFIT/ENG
U	U	U	UU	76	19b. TELEPHONE NUMBER *(Include area code)* (312) 785-3636 (x4382) (tod.laurvick@afit.edu)